Levodopa partially rescues microglial numerical, morphological, and phagolysosomal alterations in a monkey model of Parkinson's disease

Cynthia Lecours, Marie-Kim St-Pierre, Katherine Picard, Maude Bordeleau, Melanie Bourque, Ifeoluwa Oluleke Awogbindin, Amin Benadjal, Fernando González Ibanez, Dave Gagnon, Leo Cantin, et al.

Brain, Behavior, and Immunity 90 (2020) 81–96

Contents lists available at ScienceDirect

Brain, Behavior, and Immunity

journal homepage: www.elsevier.com/locate/ybrbi

Levodopa partially rescues microglial numerical, morphological, and phagolysosomal alterations in a monkey model of Parkinson's disease

Cynthia Lecours[a,b], Marie-Kim St-Pierre[a,1], Katherine Picard[a,1], Maude Bordeleau[a,c], Melanie Bourque[a], Ifeoluwa Oluleke Awogbindin[a,d], Amin Benadjal[a,e], Fernando González Ibanez[a], Dave Gagnon[f,g], Leo Cantin[a,h], Martin Parent[f,g], Therese Di Paolo[a,b,*], Marie-Eve Tremblay[a,i,j,k,*]

[a] Axe Neurosciences, Centre de Recherche du CHU de Québec-Université Laval, Québec, QC, Canada
[b] Faculté de Pharmacie, Université Laval, Québec, QC, Canada
[c] Integrated Program of Neuroscience, Faculty of Medicine, McGill University, Montréal, QC, Canada
[d] Neuroimmunology Group, Molecular Drug Metabolism and Toxicology Laboratory, Department of Biochemistry, University of Ibadan, Ibadan, Nigeria
[e] Biologie Intégrative et Physiologie, Sorbonne Université, Paris VI, France
[f] Département de Psychiatrie et de Neurosciences, Faculté de Médecine, Université Laval, Québec, QC, Canada
[g] CERVO Brain Research Center, Québec, QC, Canada
[h] Département de Chirurgie, Faculté de Médecine, Université Laval, Québec, QC, Canada
[i] Département de Médecine Moléculaire, Faculté de Médecine, Université Laval, Québec, QC, Canada
[j] Division of Medical Sciences, University of Victoria, Victoria, BC, Canada
[k] Department of Biochemistry and Molecular Biology, The University of British Columbia, Vancouver, BC, Canada

ARTICLE INFO

Keywords:
Neuroinflammation
Microglia
Basal ganglia
Parkinson's disease
MPTP monkey model

ABSTRACT

Parkinson's disease (PD) is the most common neurodegenerative motor disorder. The mechanisms underlying the onset and progression of Levodopa (L-Dopa)-induced dyskinesia (LID) during PD treatment remain elusive. Emerging evidence implicates functional modification of microglia in the development of LID. Thus, understanding the link between microglia and the development of LID may provide the knowledge required to preserve or promote beneficial microglial functions, even during a prolonged L-Dopa treatment. To provide novel insights into microglial functional alterations in PD pathophysiology, we characterized their density, morphology, ultrastructure, and degradation activity in the sensorimotor functional territory of the putamen, using 1-methyl-4-phenyl-1,2,3,6-tetrahydropyridine (MPTP) cynomolgus monkeys. A subset of MPTP monkeys was treated orally with L-Dopa and developed LID similar to PD patients. Using a combination of light, confocal and transmission electron microscopy, our quantitative analyses revealed alterations of microglial density, morphology and phagolysosomal activity following MPTP intoxication that were partially normalized with L-Dopa treatment. In particular, microglial density, cell body and arborization areas were increased in the MPTP monkeys, whereas L-Dopa-treated MPTP animals presented a microglial phenotype similar to the control animals. At the ultrastructural level, microglia did not differ between groups in their markers of cellular stress or aging. Nevertheless, microglia from the MPTP monkeys displayed reduced numbers of endosomes, compared with control animals, that remained lower after L-Dopa treatment. Microglia from MPTP monkeys treated with L-Dopa also had increased numbers of primary lysosomes compared with non-treated MPTP animals, while secondary and tertiary lysosomes remained unchanged. Moreover, a decrease microglial immunoreactivity for CD68, considered a marker of phagocytosis and lysosomal activity, was measured in the MPTP monkeys treated with L-Dopa, compared with non-treated MPTP animals. Taken together, these findings revealed significant changes in microglia during PD pathophysiology that were partially rescued by L-Dopa treatment. Albeit, this L-Dopa treatment conferred phagolysosomal insufficiency on microglia in the dyskinetic Parkinsonian monkeys.

* Corresponding authors at: CHU de Québec-Université Laval, 2705, Boulevard Laurier, Québec, QC G1V 4G2, Canada (T. Di Paolo). Division of Medical Sciences, University of Victoria, Medical Sciences Building, room 322, Victoria, BC V8P 5C2 Canada (M.-E. Tremblay).
E-mail addresses: therese.dipaolo@crchudequebec.ulaval.ca (T. Di Paolo), evetremblay@uvic.ca (M.-E. Tremblay).
[1] These authors contributed equally.

https://doi.org/10.1016/j.bbi.2020.07.044
Received 11 April 2020; Received in revised form 23 July 2020; Accepted 29 July 2020
Available online 02 August 2020

1. Introduction

Parkinson's disease (PD) is the second most prevalent neurodegenerative disorder after Alzheimer's disease (Lebouvier et al., 2009). About 1% of the worldwide population above 60 years of age is affected by PD (Morin et al., 2014; Tysnes and Storstein, 2017). PD is thought to result from an interplay between genetic variations and various risk factors such as aging, chronic stress, brain trauma, and infection (Tansey and Goldberg, 2010; Schapira and Jenner, 2011; Vyas et al., 2016; Niraula et al., 2017). Signs of rigidity, bradykinesia, resting tremors, and postural instability allow clinical diagnosis of the disease (Jankovic, 2008). The motor deficits in PD emerge from a progressive degeneration of *substantia nigra* (SN) *pars compacta* dopaminergic (DA) neurons. These DA neurons innervate the striatum, including the sensorimotor putamen, which is involved in long-term representation of motor sequences (Lehéricy et al., 2005). DA neuronal degeneration leads to a significant decrease of DA content in the striatum (Morin et al., 2014; Tysnes and Storstein, 2017).

Despite lacking a disease-modifying property, treatment with Levodopa (L-Dopa), a natural precursor of DA, combined with a Dopa decarboxylase inhibitor, which prevents L-Dopa degradation in the periphery, provides an effective symptomatic relief (Mercuri and Bernardi, 2005; Poewe et al., 2010; Montioli et al., 2016). However, as the disease progresses, beneficial effects of L-Dopa become associated with, as early as five years into treatment, with first into involuntary motor fluctuations and later L-Dopa-induced dyskinesia (LID) (Barnum et al., 2008; Martinez et al., 2015). Indeed, most patients experience abnormal involuntary movements caused by L-Dopa treatment that can be more debilitating than PD itself (Ahlskog and Muenter, 2001; Mercuri and Bernardi, 2005; Fabbrini et al., 2007). This suggests that the blunting of clinical improvement during L-Dopa treatment may be associated with disruptive neurochemical changes and/or progressive dysfunction of cellular mediators over time. Regrettably, after > 40 years of clinical use, alternatives to L-Dopa treatment are still limited. People with PD now live longer (ever-increasing disease duration) and are chronically exposed to DA treatment that can lead to LID. Therefore, LIDs remain a challenge in PD treatment, despite the scientific knowledge advent and a recent, but controversial, review on the decline of troublesome dyskinesia prevalence due to better management of PD (Chaudhuri et al., 2019). Available therapeutics that can improve LID and other L-Dopa associated complications, without loss of therapeutic efficacy, remain an unmet need (Vijayakumar and Jankovic, 2016). Amantadine, an anti-viral agent and a glutamate NMDA receptor antagonist (e.g., new ADS-5102), is the most prescribed anti-LID drug but it is associated with debilitating side-effects (Hubsher et al., 2012; Pahwa et al., 2015, 2017; Hauser et al., 2017; Oertel et al., 2017). Clozapine is another anti-LID drug but with potential serious adverse effects (e.g., agranulocytosis) (Durif et al., 2004). Thus, elucidating the neuropathological events underlining LID may bring us a step closer to developing an effective therapy to manage LID in the foreseeable future.

LID occur when the levels of DA in the striatum are too high, very low or persistently unstable (Huot et al., 2013). As such, symptomatic motor deterioration during L-Dopa treatment is partly attributed to the progressive loss of striatal DA axon terminals, which convert L-Dopa to DA, as well as loss of DA transporter on DA terminals (Hong et al., 2014). This culminates in an abnormal activation of DA receptors at the synapses of dorsolateral putamen (Carta et al., 2017). However, emerging evidence suggest indirect contributions of L-Dopa in the onset and severity of LID through non-neuronal mechanisms involving alterations of neurochemicals as well as microglia, the immune cells of the brain (Carta et al., 2017). For instance, 6-hydroxydopamine (6-OHDA)-lesioned rats affected with LID presented exacerbated levels of the pro-inflammatory cytokines tumor necrosis factor (TNF)-α and interleukin (IL)-1β in the striatum (Barnum et al., 2008; Mulas et al., 2016). In this animal model, treatment with anti-inflammatory drugs, such as corticosterone and the PPAR-γ agonist rosiglitazone, attenuated both the intensity of LID and the levels of pro-inflammatory cytokines in the striatum (Barnum et al., 2008; Martinez et al., 2015). Intrastriatal infusion of the IL-1β receptor antagonist, IL-1ra, was also sufficient to decrease LID severity, which supports a local action of the pro-inflammatory cytokine (Barnum et al., 2008). Similarly, peripheral lipopolysaccharides (LPS; bacterial component) administration increased LID in 6-OHDA-lesioned hemiparkinsonian rats (Mulas et al., 2016). In this study, LID was associated with increased brain levels of TNFα without significant changes in the periphery. Of note, the anti-dyskinetic drug amantadine attenuated microglial secretion of TNF-α and nitric oxide following LPS challenge in a neuron-microglia co-culture (Ossola et al., 2011; Kim et al., 2012). The study further speculates against the conventional belief that the neuroprotective potential of amantadine is microglial-dependent but independent from NMDA receptor inhibition. This is because at lower concentration, amantadine protects neuron-glia culture from 1-methyl-4-phenylpyridinium (MPP^+) and LPS-induced toxicity whereas higher concentration of 4–5 folds was required to resolve NMDA-induced toxicity. Also, evidence from a non-human primate model of PD and *post-mortem* PD brains receiving L-Dopa treatment revealed a significantly reduced level of arachidonic acid, a precursor of several pro-inflammatory prostaglandins, in non-dyskinetic subjects compared with those displaying motor complications (Julien et al., 2006). Taken together, microglia-mediated neuroinflammation might contribute significantly to LID. Understanding the link between microglial functional capacity and the pathophysiology of PD including the development of LID is thus crucial to determine their contributions to LID. This may provide a template for microglial rejuvenation or restoration of beneficial functions, even during a prolonged L-Dopa treatment (Awogbindin et al., 2020).

Even though the direct contribution of L-Dopa to progressive nigrostriatal neurodegeneration is being debated (Fahn et al., 2004; Lipski et al., 2011), increased concentration of extrasynaptic DA in the cytosol, which characterizes chronic non-physiological DA supplementation during L-Dopa treatment, may fuel the accumulation of toxic metabolites and oxidative stress (Sabens et al., 2010; Lipski et al., 2011) with deleterious outcomes on the surrounding microglia. For instance, unutilized L-Dopa and DA auto-oxidize to reactive quinones, semiquinones, aminochromes or a more stable neuromelanin (Kostrzewa et al., 2002; Herrera et al., 2017). These metabolites form covalent complexes with alpha (α)-synuclein (Fasano et al., 2003; Xu and Chan, 2015), a dysfunctional signal that fuels pro-inflammatory microglial phenotypic switch and impairment of phagocytosis (Choi et al., 2015; Awogbindin et al., 2020). Moreover, the degeneration of neurons containing neuromelanin overload may further solicit microglial involvement and trigger pro-inflammatory responses (Zecca et al., 2008; Zhang et al., 2011; Viceconte et al., 2015). Importantly, using mouse-derived microglia deficient in macrophage antigen complex-1, a receptor involved in phagocytosis initiation, Zhang et al. demonstrated that microglial phagocytosis of neuromelanin contributes to the degeneration of primary ventral midbrain neurons in culture (Zhang et al., 2011). Thus, we hypothesize that microglial intracellular machineries involved in debris clearance may particularly become compromised during LID.

To study the implications of microglia in PD pathophysiology including the development and expression of LID, we have characterized the changes in their density, morphology, ultrastructure, as well as degradation activity in the sensorimotor putamen of 1-methyl-4-phenyl-1,2,3,6-tetrahydropyridine (MPTP) cynomolgus monkeys (*Macaca fascicularis)*. The MPTP monkey model best replicates the emergence of LID symptoms upon L-Dopa treatment (Morin et al., 2014). Using a combination of light, confocal, and transmission electron microscopy, our analyses in MPTP monkeys compared with healthy controls first revealed increases in microglial density, as well as cell body and process arborization area, that returned to control values with L-Dopa treatment. These changes indicate that microglia become

more numerous and hyper-ramified in the striatum of MPTP monkeys, while their phenotypic changes are normalized by L-Dopa. At the ultrastructural level, microglia did not show signs of cellular stress and/or early aging (e.g. dilation of the Golgi apparatus and endoplasmic reticulum, accumulation of lipofuscin granules) in the different groups. However, microglia from MPTP monkeys, without or with L-Dopa treatment, displayed decreased numbers of endosomes compared to control animals. Microglia from MPTP animals treated with L-Dopa also had increased numbers of primary lysosomes, which might reflect a compensatory mechanism, while secondary and tertiary lysosomes remained unchanged in number. In addition, microglial immunoreactivity for CD68, a glycoprotein associated with their phagolysosomal activity, was unchanged at the confocal level after MPTP exposure, but decreased with L-Dopa treatment. While CD68 is considered a marker of phagocytosis and lysosomal activity, we provide ultrastructural evidence that it localizes to secondary lysosomes, in which endosomes are fused to lysosomes, as well as tertiary residual debris in striatal microglia. Overall, these findings identify striatal microglial changes that are partially rescued by L-Dopa treatment during PD pathophysiology. In addition, our study reveals for the first time a phagolysosomal insufficiency in microglia during LID. Therapeutic interventions targeting microglial reactivity, specifically their dysfunctional phagolysosomal activity, may prove invaluable in the prevention of L-Dopa associated abnormal involuntary movements.

2. Material and methods

2.1. Animal model

2.1.1. Statement on the welfare of animals

All experimental procedures were approved by the *Comité de protection des animaux de l'Université Laval* (protocols # 2010–062 and 2015–089), according to the Canadian Council on Animal Care's Guide to the Care and Use of Experimental Animals (Ed2) guidelines. Minimal number of animals were used in these experiments.

2.1.2. Experimental groups

This study was conducted on 12 ovariectomized adult female monkeys (*Macaca fascicularis*, Primus Bio-Resources, Charles River) between 4 and 11 years of age that weighed between 2.8 and 4.6 kg (Table 1). Animals were housed under a 12-hour light–dark cycle with water and food provided *ad libitum*.

Four monkeys were used as controls and 8 others received systemic infusion of MPTP (Sigma-Aldrich) through subcutaneous Alzet minipumps (0.5 mg/24 h in saline solution; Durect Corporation) until stabilization of the bilateral parkinsonian syndrome was achieved (Riahi et al., 2013). Behavioral response to MPTP intoxication was assessed by using a motor scale developed at Université Laval that takes into consideration posture, mobility, climbing, gait, grooming, voicing, social interaction and tremor (Hadj Tahar et al., 2004). Animals were scored twice, one week before transcardiac perfusion, using 2 h video recording sessions during which behavior was scored every 15 min. At the time of perfusion, all MPTP monkeys were stabilized and did not show any sign of behavioral recovery. Four of the eight MPTP monkeys received chronic L-Dopa to model LID. These monkeys were treated chronically, during a one month-period or until dyskinesia stabilized, once daily with L-Dopa/benserazide 100/25 mg capsule p.o. alone (Prolopa, Hoffmann-La Roche; a mixture of 100 mg of L-Dopa and 25 mg of benserazide). Afterwards, behavioral responses were video recorded for each animal following a subcutaneous administration of L-Dopa methyl ester (Sigma-Aldrich) at a fixed dose (15–30 mg/kg), tailored for each animal for an optimal response, always in combination with benserazide (50 mg, Sigma-Aldrich), a peripheral Dopa decarboxylase inhibitor. The behavioral responses of each MPTP animal were video recorded in the morning after a subcutaneous injection of vehicle (saline solution) (for 2–3 h) and on another day in the morning following administration of L-Dopa (for 4–5 h, i.e. duration of the motor response). Video analysis was conducted blind to the experimental conditions. All MPTP and MPTP + L-Dopa animals were scored using a motor scale that distinguishes between mild, moderate or severe parkinsonism, and MPTP + L-Dopa animals using the dyskinetic scale quantifying LID, as described previously (Hadj Tahar et al., 2004). The dyskinetic score measures the severity of dyskinesias. The difference between mild, moderate and severe dyskinesias for a given body segment is based on the assessment of the amplitude and frequency (whether they are occasional, intermittent, or constant) of abnormal movements. For the microglial analyses, monkeys were matched for their parkinsonian score and had a similar extent of denervation as shown in Fig. 1A (disability scale, showing the parkinsonian score) and extent of denervation as shown in Fig. 1C (estimated with DA transporter (DAT) immunostaining). All animals (Table 1) were used for light, confocal and transmission electron microscopy, except for S2711 which did not have an optimal ultrastructural preservation and was not used for transmission electron microscopy. An additional MPTP monkey, 4 years of age, was also used to determine the subcellular localization of CD68 in the sensorimotor territory of the putamen.

Table 1
Information on the control, MPTP and MPTP + L-Dopa treated female monkeys used for this study.

Group	ID	Weigth (kg)	Age (year)	Survival time post-MPTP (year)
Control	S-2310	3.9	4.33	
	S-2311	3.0	4.25	
	S-2312	3.5	3.83	
	S-2313	3.8	4.5	
Mean ± S.E.M.	–	3.6 ± 0.20	5.23 ± 0.14	–
MPTP	S-2268	3.2	5.1	0.33
	S-2269	3.1	5	0.18
	S-2270	2.8	5	0.15
	S-2273	3.3	5.1	0.20
Mean ± S.E.M.	–	3.1 ± 0.11	5.05 ± 0.03	0.22 ± 0.04
MPTP + L-Dopa	S-2631	4.6	11.2	7.21
	S-2711	2.9	9.75	1.67
	S-2722	3.5	9	0.51
	S-2747	3.7	10.3	1.25
Mean ± S.E.M.	–	3.7 ± 0.35	10.06 ± 0.46 *,†	2.66 ± 1.54

NOTE: * $p < 0.0001$ *vs* Control monkeys; † $p < 0.0001$ *vs* MPTP monkeys

2.1.3. Tissue processing

Following behavioral scoring, the animals were euthanized and brain tissues were collected using a technique compatible with both immunohistochemistry and electron microscopy as described in (Tremblay et al., 2010b). One monkey was excluded from the ultrastructural analysis, only keeping those with an optimal brain tissue preservation (4 controls, 4 MPTP, and 3 MPTP + L-Dopa). Monkeys were first anesthetized with a cocktail of ketamine (20 mg/kg, i.m.) and xylazine (4 mg/kg, i.m.) and were maintained under anesthesia using 3% isoflurane. For perfusion, 300 mL of ice-cold sodium phosphate-buffered saline (PBS, 0.1 M; pH 7.4) was administered transcardially, followed by 1 L of cold 4% paraformaldehyde (PFA) mixed with 0.1% glutaraldehyde and finally by 1.5 L of 4% PFA. Brains were then post-fixed for 24 h at 4°C in 4% PFA. The next day, 50 µm-thick brain sections were cut in PBS using a vibratome (VT1200 S; Leica). Afterwards, sections were stored in cryoprotectant (30% ethylene glycol and 30% glycerol in PBS) at −20°C.

2.2. Immunohistochemistry staining

2.2.1. Light microscopy

To measure microglial density and morphology, 7 rostrocaudal sections were selected across the entire striatum of each monkey, at a fixed interval of 600 µm. The sections were immunostained using the

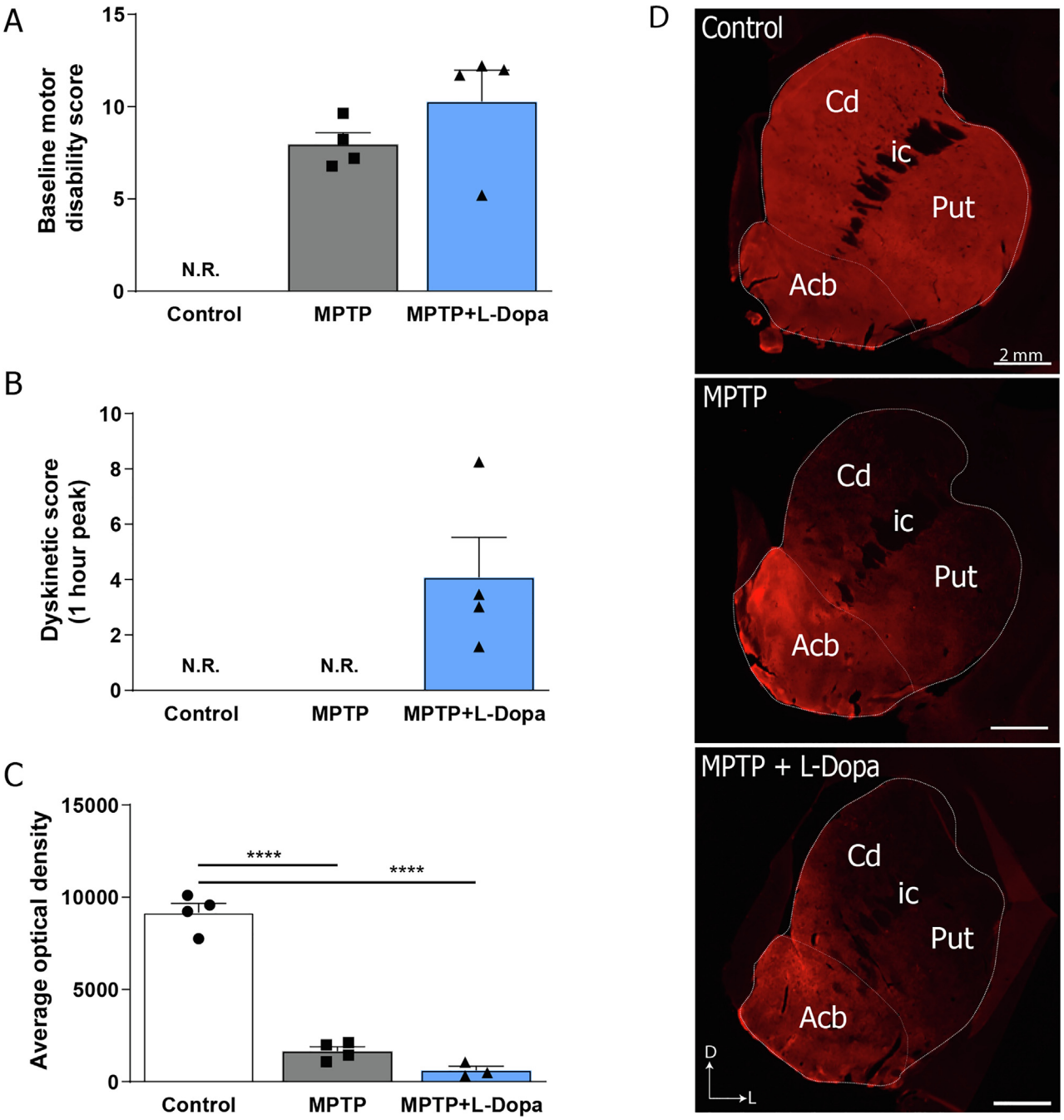

Fig. 1. Effects of MPTP treatment on motor behavior and DAT staining in the striatum of macaque monkeys. A-C: Histograms showing the (A) motor disability score at baseline (MPTP monkeys: S-2268: 8.23, S-2269: 9.64, S-2270: 6.78 and S-2273: 7.20 and MPTP + L-Dopa treated monkeys: S-2631: 12.00, S-2711: 5.21, S-2722: 12.22 and S-2747: 11.72), (B) dyskinetic score at the 1 h peak (MPTP + L-Dopa treated monkeys: S-2631: 3.47, S-2711: 1.58, S-2722: 3.02 and S-2747: 8.25) and (C) average optical density of the DAT immunostaining. D: Representative images of DAT immunostaining in the striatum of control, MPTP-intoxicated and MPTP-treated with L-Dopa monkeys. Data shown are expressed as means ± S.E.M. **** $p < 0.0001$, by using one-way ANOVA followed by a Bonferroni *post-hoc* test. Acb: *nucleus accumbens*; Cd: caudate nucleus; ic: internal capsule; N.R.: not relevant; Put: putamen. Scale bars: 2 mm.

marker ionized calcium binding adaptor molecule 1 (IBA1) to analyze microglia at the light microscopy level. Cryoprotectant was rinsed out with PBS and the free-floating sections were quenched with 2% H_2O_2 in 70% methanol for 5 min, and then washed with PBS (50 mM at pH 7.4). They were then placed in 0.1% $NaBH_4$ solution for 30 min and washed. Tissues were incubated in a blocking solution containing 10% fetal bovine serum (FBS), 3% bovine serum albumin (BSA) and 1% Triton X-100 for 1 h at room temperature (RT). They were then incubated overnight at 4°C in rabbit anti-IBA1 primary antibody (1:1000 in blocking solution; catalog no. 019–19741; Wako). The following day, after several washes with Tris-buffered saline (TBS; 50 mM at pH 7.4), sections were incubated in goat anti-rabbit biotin-conjugated secondary antibody (1:200 in TBS; catalog no. 111–066-046; Jackson ImmunoResearch) for 1.5 h at RT. The sections were incubated 1 h with avidin–biotin-peroxidase complex (ABC; 1:100 in TBS; Vector Laboratories). They were rinsed and developed using diaminobenzidine (DAB; 0.05%) and H_2O_2 0.015% in Tris buffer (TB; 50 mM at pH 8.0) for 4 min at RT. Sections were mounted on charged glass slides. They were dehydrated in increasing concentrations of ethanol (2 min for each concentration). Slides were then submerged in CitriSolV (catalog no

1601; Decon Laboratories) and coverslipped with dibutylphthalate polystyrene xylene (DPX) (Electron Microscopy; EMS).

2.2.2. Fluorescent microscopy

Immunochemistry for DAT was performed to evaluate the extent of the DA lesion caused by MPTP intoxication. Transverse sections were taken through 3 striatal levels, pre-commissural (3.0 mm), commissural (0.0 mm) and post-commissural (-3.0 mm), according to the brain stereotaxic atlas of Martin and Bowden (Martin and Bowden, 2000). These sections were immunostained for DAT with secondary antibodies coupled to an infrared fluorescent dye. Briefly, sections were first washed in PBS (50 mM at pH 7.4), then incubated at RT for 1 h in a blocking solution containing 1% Triton X-100 and 2% normal goat serum (NGS) in PBS. Afterward, sections were incubated overnight at 4°C in the same blocking solution to which a 1:500 dilution of rat anti-DAT (product no. MAB369; EMD Millipore Corporation) was added. After being rinsed in PBS, sections were incubated with goat anti-rat IRDye 800CW (catalog no. 926–32219; LI-COR Biosciences) diluted 1:1000 in the blocking solution, for 2 h at RT. An infrared imaging system (Odyssey CLx; LI-COR Biosciences) was then used to scan the immunostained sections and measurements were taken from the 3 functional territories of the striatum, as defined according to Parent and Hazrati (Parent and Hazrati, 1995). Secondary antibody was excited with the appropriate solid-state diode laser (785 nm).

To evaluate microglial phagolysosomal function, IBA1/CD68 double staining was performed. Two rostrocaudal sections (3.0 mm to −3.0 mm) per animal were selected. They were quenched with 0.5% $NaBH_4$ for 30 min and then blocked with a mixture of 2% normal donkey serum (NDS), 2% NGS and 0.3% Triton X-100 (in PBS) for 1 h. Combined primary antibodies: rabbit anti-IBA1 antibody (1:1000, catalog no. 019–19741; Wako) and mouse anti-CD68 antibody (1:50, catalog no. M0814; Dako) were incubated overnight at 4°C in blocking solution. The next day, sections were incubated with goat anti-rabbit Alexa Fluor 488-conjugated (1:300, catalog no. A-11008; Thermo-Scientific) and donkey anti-mouse Alexa Fluor 568-conjugated (1:300, catalog no. A-10037; Thermo-Scientific) secondary antibodies in blocking buffer for 2 h at RT. Sections were washed in PBS, counterstained with DAPI for 5 min, mounted on slides and coverslipped with Fluoromount-G (catalog no. 0100–01; SouthernBiotech).

To quantify the circulating monocytes infiltrating the sensorimotor region of the dorsal putamen, an IBA1/TMEM119 double staining was also performed. The marker IBA1 is commonly used to study microglia, considering that it provides an exceptional visualization of their morphology (González Ibanez et al., 2019), but it is also expressed by peripheral myeloid cells that can infiltrate the brain, especially in contexts of disease, while TMEM119 is considered to be microglia-specific (Bennett et al., 2016). One rostrocaudal section per animal (3.0 mm to −3.0 mm) was quenched with 0.1% $NaBH_4$ for 30 min and then blocked with a mixture of 5% NDS, 0.5% gelatin and 0.3% Triton X-100 (in TBS) for 1 h. The sections were incubated with rabbit anti-TMEM119 primary antibody (1:500, catalog no. HPA051870; Sigma-Aldrich) overnight at 4°C. The next day, the sections were washed and incubated with donkey anti-rabbit Alexa Fluor 568-conjugated secondary antibody (1:300, catalog no. A-10042; Thermo-scientific) for 2 h at RT, and then with rabbit anti-IBA1 primary antibody conjugated to Alexa Fluor 635 (1:100, catalog no. 013–26471; Fujifilm Wako) overnight at 4°C. All the antibodies were diluted in blocking buffer. The next day, the sections were washed in PBS, counter-stained with DAPI, mounted on slides and coverslipped with Fluoromount-G.

2.2.3. Electron microscopy

For transmission electron microscopy, two rostrocaudal transverse sections taken at the commissure level (0.0 mm) were selected for each of the 11 monkeys used in the ultrastructural analysis. They were immunostained for IBA1 to analyze microglial ultrastructural features. Cryoprotectant was first rinsed out with PBS and free-floating brain sections were quenched with 0.3% (v/v) H_2O_2 in PBS for 5 min followed by a 30 min incubation in 0.1% $NaBH_4$. For blocking, sections were incubated in 10% FBS, 3% BSA and 0.01% Triton X-100 for 1 h at RT. They were then incubated overnight at 4°C in rabbit anti-IBA1 primary antibody (1:5000, catalog no. 019–19741; Wako) diluted in blocking solution. The following day, sections were incubated in donkey anti-rabbit biotin-conjugated secondary antibody (1:300 in TBS; catalog no. 111–066-046; Jackson ImmunoResearch) for 1.5 h, ABC for 1 h, and the staining was revealed with 0.05% DAB and 0.015% H_2O_2 during 4 min at RT. Sections were then incubated in 1% osmium tetroxide for 30 min. After washes with phosphate buffer, sections were dehydrated in increasing concentrations of ethanol, followed by 3 washes of 5 min in propylene oxide and immersion in Durcupan resin (Electron Microscopy Sciences; EMS) for 24 h at RT. The next day, sections were flat-embedded between ACLAR sheets (EMS) and resin was polymerized at 55°C for 72 h. In each section, a trapezoid was excised from the sensorimotor territory of the putamen and re-embedded on a resin block. Ultrathin sections, approximately 75 nm-thick, were cut with an ultramicrotome (Leica Ultracut UC7) and collected on copper 200-mesh grids (EMS).

Immunostaining against CD68 was also performed to determine its subcellular localization in microglia using transmission electron microscopy, using one transverse section taken at the commissure level from one animal, as for the IBA1 staining. Tissues were quenched with 0.3% H_2O_2 in PBS for 5 min, then placed in 0.1% $NaBH_4$ for 30 min. Sections were incubated overnight at 4°C with a mouse anti-CD68 primary antibody (1:50, catalog no. M0814; Dako) in blocking solution (10% FBS, 5% BSA and 0.01% Triton X-100). The next day, sections were incubated in goat anti-mouse biotin-conjugated secondary antibody (1:300 in 0.01% Triton X-100 added to TBS; catalog no. 115–066-071; Jackson ImmunoResearch) for 1.5 h. The following steps were identical to the ones described above for IBA1 except that 0.01% Triton X-100 in TBS was used to wash sections.

2.3. Microscopy analyses

2.3.1. Microglial density and morphology analyses

To analyze microglial density, an unbiased stereological approach was performed using a light microscope equipped with the StereoInvestigator software (v. 7.00.3; MicroBrightField), a digital camera with a motorized stage and a Z-axis indicator. Using the stereotaxic atlas of Martin and Bowden (Martin and Bowden, 2000), the contour of the sensorimotor functional territory of the putamen was traced at a low magnification on each transverse section, according to Parent and Hazrati (1995). A grid composed of 1500 X 1500 µm squares was randomly placed over the contour and a counting frame of 200 X 200 µm was drawn at each intersection of the grid. Every IBA1-immunopositive cell body contained inside of the counting frame that did not touch the exclusion lines was counted at a magnification of 100X. For each counting frame, thickness of the brain section was determined. The mean section thickness was 24.3 ± 2.1 µm. Coefficients of error (Gunderson, $m = 1$ and 2nd Schmitz-Hof) obtained were 0.03 or 0.04, respectively.

For the analysis of microglial morphology, colored pictures were acquired at 40X using a Zeiss AxioPlan brightfield microscope equipped with an Infinity 2 camera (5 MP; Lumenera). An observer blinded to the experimental groups analyzed the images. For each animal, 15 IBA1-immunopositive cell bodies and their arborizations were analyzed using ImageJ software (NIH, v.1.50b). All the cells in focus were analyzed in each picture before moving to the next picture not to introduce selection bias (Tremblay et al., 2012). For each cell, the soma area was determined by tracing a line around the cell body using the freehand selection tool of ImageJ. Distal process extremities were also connected together to measure arborization area using the polygon selection tool of ImageJ. A morphological index was next calculated by dividing the soma area by the arborization area (Milior et al., 2016) in order to

Table 2
Additional results from the ultrastructural analyses of IBA1-positive cell bodies. All analyzed features are expressed as numbers/cell body.

	Mean ± SEM		*P* value
	Control	MPTP	
Lipofuscin	0.05405 ± 0.03769	0.1053 ± 0.06299	0.7399
ER and Golgi dilation	0.4595 ± 0.1429	0.2105 ± 0.09359	0.2255
Elongated mitochondrion	0.08108 ± 0.04549	0.1579 ± 0.07082	0.8697
Extracellular digestion	0.6486 ± 0.1239	0.7368 ± 0.1586	> 0.9999
Extracellular space pocket	0.7027 ± 0.07618	0.7895 ± 0.06702	0.7255
Synaptic contact	1.243 ± 0.1875	0.9211 ± 0.1380	0.2807
	Mean ± SEM		*P* value
	MPTP	MPTP + L-Dopa	
Lipofuscin	0.1053 ± 0.06299	0.1111 ± 0.06163	0.9967
ER and Golgi dilation	0.2105 ± 0.09359	0.1481 ± 0.08777	> 0.9999
Elongated mitochondrion	0.1579 ± 0.07082	0.3333 ± 0.1068	0.2070
Extracellular digestion	0.7368 ± 0.1586	0.6296 ± 0.1524	> 0.9999
Extracellular space pocket	0.7895 ± 0.06702	0.8889 ± 0.06163	0.6775
Synaptic contact	0.9211 ± 0.1380	0.7037 ± 0.1393	0.7195

determine microglial reactivity (Streit et al., 1999). This morphological index was used to correlate the area of the soma with the area of the arborization; the larger the value is, the greater the soma is compared to the ramifications.

2.3.2. Microglial ultrastructural analyses

Between 7 and 10 IBA1-positive cell bodies in each of the 11 examined animals (4 control, 4 MPTP and 3 MPTP + L-Dopa monkeys) were randomly acquired at 6800X using a FEI Tecnai Spirit G2 transmission electron microscope operating at 80 kV and equipped with a digital camera ORCA-HR (10 MP; Hamamatsu). The images were analyzed with ImageJ by an observer blinded to the experimental conditions. For each cell body, the number of lysosomes, lipofuscin granules, dilated endoplasmic reticulum (ER) and Golgi apparatus cisternae, endosomes (either empty or containing debris), elongated mitochondria, extracellular digestion events, and contacts made onto synaptic elements (dendritic spines recognized by their post-synaptic density, axon terminals identified by their synaptic vesicles) were analyzed, as previously described (St-Pierre et al., 2019). Lipofuscin granules were identified by their dark heterogeneous and granulous appearance (Peters et al., 1991). Endosomes were identified by their ovoid shape delineated by a single membrane. They contained partially or fully digested cellular constituents such as vesicles and myelin debris. Their size had to be between 100 nm and 1.7 μm for inclusion in the analysis. Lysosomes were identified by their dark appearance, size between 0.5 μm and 2.0 μm, and frequent association with degraded lipid bodies or vacuoles (El Hajj et al., 2019). Primary, secondary and tertiary lysosomes were differentiated based on the criteria previously established by El Hajj et al. (El Hajj et al., 2019). Briefly, primary lysosomes were characterized by their round homogenous shape with electron-dense granules found near the membrane. Secondary lysosomes were identified based on their round heterogenous and electron-dense shape, as well as their association with vacuoles, while tertiary lysosomes were differentiated from secondary lysosomes by their association with vacuoles, lipofuscin granules and lipid bodies. Cisternae of ER and Golgi apparatuses had a minimum width of 50 nm to be considered dilated. Mitochondria had to be at least 1000 nm of length to be considered elongated (Hui et al., 2018). Elongated mitochondria were previously associated with a shift in the fusion/fission balance towards fusion (Westermann, 2008). Microglia-associated extracellular space pockets were larger than the extracellular space usually observed between neighboring cells (Tremblay et al., 2010a) and were distinguished from distal astrocytic processes by their lack of a delineating plasma membrane (Peters et al., 1991). Extracellular digestion, which is also termed "exophagy" (Haka et al., 2016; El Hajj et al., 2019), was identified as extracellular space pockets containing partially digested cellular elements such as membranes sometimes forming myelin, axon terminals or dendritic spines.

2.3.3. Peripheral myeloid cell infiltration and phagolysosomal activity analyses

Confocal imaging of the IBA1/CD68 double staining was performed using an inverted Leica DMI 600B microscope with a Quorum WaveFX Spinning disk. Images of the sensorimotor putamen were captured at a magnification of 40X with the 491 nm (green) and 561 nm (red) lasers. Z-stacks were acquired using a Hamamatsu ORCA-R2 camera (512 X 512 pixels). Merged planes pictures were generated from the z-stacks using Volocity software (Version 5.4, PerkinElmer). Confocal imaging of the IBA1/TMEM119 double staining was performed using a Zeiss Axio Imager Z2 microscope. Images of the sensorimotor putamen were captured at a magnification of 20X using the 561 nm (red) and 640 nm (far red) lasers. Z-stacks were acquired with an Axiocam 506 mono camera. The analyses of the double staining were performed blind to the experimental conditions using either Photoshop CC 2018 (IBA1/CD68) or ImageJ (IBA1/TMEM119). Between 30 and 50 IBA1-immunopositive microglial cells per animal were randomly analyzed for colocalization with CD68 or TMEM119, in both cell body and processes. Every IBA1-immunopositive cells not touching the exclusion lines, as for the density analysis, were examined to avoid selection bias. For CD68, puncta smaller than 2 pixels were excluded.

2.4. Statistical analyses

All statistical analyses were conducted using GraphPad Prism software (v. 6.01). A parametric one-way ANOVA test was performed and followed by a Bonferroni *post-hoc* test to make specific comparisons between the groups: control *vs* MPTP, MPTP *vs* MPTP + L-Dopa, and control *vs* MPTP + L-Dopa for Table 1 and Fig. 1, or control *vs* MPTP and MPTP *vs* MPTP + L-Dopa for Table 2 and all the other figures. An unpaired Student's *t*-test was instead used when comparing only two groups, for the survival time post-MPTP (Table 1) and motor disability score (Fig. 1A). To identify statistically significant outliers, an online Grubbs test (GraphPad Prism; https://www.graphpad.com/quickcalcs/Grubbs1.cfm) was used in all the experiments and the outliers were removed from the datasets. Sample size (n) refers to the number of animals used for the motor disability and dyskinetic scores, DAT analysis, as well as IBA1-positive cells for density experiments, or to the number of IBA1-positive cells examined in the other experiments, as previously published by our group (Milior et al., 2016; Hui et al., 2018; El Hajj et al., 2019). Differences were considered statistically significant at $p < 0.05$. All reported values are mean ± standard error of the mean (S.E.M.).

3. Results

3.1. MPTP monkeys display motor disability as well as dyskinesia upon L-Dopa treatment

After behavioral stabilization subsequent to MPTP administration, the motor behavior of all MPTP monkeys used in the present study was assessed under basal conditions, following administration of vehicle. The baseline motor disability scores did not differ significantly between the two MPTP monkey groups (Fig. 1A $p = 0.4124$), indicating a similar parkinsonian syndrome under basal conditions. The L-Dopa treated MPTP group also developed moderate LID (Fig. 1B).

3.2. MPTP monkeys show significant dopaminergic lesions regardless of L-Dopa treatment

The optical density of DAT immunostaining within the functional territories of the striatum was measured using an infrared imaging system to assess the extent of the dopaminergic lesion caused by MPTP intoxication. Both the non-treated and the L-Dopa-treated MPTP monkeys showed significantly reduced DAT immunoreactivity in the sensorimotor putamen when compared to the control group (1658 ± 241 and 624 ± 223, compared to 9166 ± 504; $p < 0.0001$) (Fig. 1C). These measures correspond to 81.9 ± 2.6% and 93.2 ± 2.4% decreases for the MPTP and MPTP + L-Dopa groups, respectively. No significant difference was found regarding the extent of MPTP-induced DA denervation between non-treated and L-Dopa-treated animals ($p = 0.2805$).

3.3. The numerical and morphological changes of microglia in the striatum of PD monkeys are normalized by L-Dopa treatment

To identify possible functional alterations of microglia during PD pathophysiology, including LID, we performed a thorough density and morphological analysis of IBA1-immunolabeled cells using light microscopy.

First, microglial density was assessed using an unbiased stereological approach by counting IBA1-immunopositive cells in the sensorimotor region of the putamen across the different experimental groups (Fig. 2). Microglial density was found to be increased in MPTP *versus* control monkeys (9190 ± 320 cells/mm^3 in MPTP *versus* 6922 ± 580 cells/mm^3 in control animals, $p = 0.0126$) (Fig. 2E). Microglial density was also normalized to control levels in MPTP monkeys treated with L-Dopa (6928 ± 376 cells/mm^3 in L-Dopa) (Fig. 2E). A double immunofluorescent staining for IBA1 (marker of myeloid cells including microglia) and TMEM119 (microglia-specific; (Bennett et al., 2016)) was then used to determine if this increase in density could result from an infiltration of circulating monocytes in the striatum (Supplementary Fig. 1). This analysis revealed that the proportion of cells only positive for IBA1 increases in the sensorimotor region of the putamen of MPTP *versus* control monkeys (7.826 ± 1.775% in MPTP *versus* 2.927 ± 1.180% in control animals, $p = 0.0159$) (Supp. Fig. 1J), suggesting that monocytic infiltration is partially responsible for the increase in IBA1-positive cell density. This proportion further reduced to control levels in MPTP monkeys treated with L-Dopa (Supp. Fig. 1J).

Microglial morphology was next examined, and morphological changes were quantified for both cell bodies and process arborization (Fig. 3). The cell body area of IBA1-positive cells was significantly increased in MPTP monkeys compared with controls (41.2 ± 1.6 μm^2 in MPTP *versus* 32.4 ± 1.0 μm^2 in control animals, $p < 0.0001$) and returned to control values in the MPTP monkeys that received L-Dopa (32.6 ± 1.3 μm^2 in L-Dopa) (Fig. 3D). The arborization area of IBA1-positive cells was also significantly increased in the MPTP group compared to control animals (1616.9 ± 53.1 μm^2 in MPTP *versus* 1454.1 ± 32.4 μm^2 in control animals, $p = 0.0140$) and normalized by the L-Dopa (1300.3 ± 41.5 μm^2 in L-Dopa animals) (Fig. 3E). In addition, the morphological index, considered a measure of microglial reactivity to injury or pathological challenges (Streit et al., 1999), was significantly increased in MPTP monkeys compared with the controls (0.027 ± 0.001 for MPTP *versus* 0.023 ± 0.001 for control animals, $p = 0.0063$) (Fig. 3F). Overall, these findings indicate that microglial density, as well as cell body and arborization areas, are increased in the striatum of MPTP monkeys, while L-Dopa treatment rescues these phenotypic alterations. These changes in microglial density and morphology might impact their physiological functions.

3.4. The phagolysosomal system of microglia is altered in the striatum of PD monkeys and partially rescued by L-Dopa treatment

To provide functional insights into the consequences of these changes in microglial density and morphology in the striatum of our PD monkey model, we next conducted ultrastructural analyses of IBA1-positive cells. Our observations did not reveal the occurrence of degenerating elements in the sensorimotor putamen of MPTP monkeys (data not shown), which is in agreement with their stable motor impairment or PD score. Microglial cellular functions were also assessed in the sensorimotor putamen, comparing controls with MPTP monkeys, and MPTP monkeys treated with L-Dopa (Fig. 4). The quantitative analysis of IBA1-positive cell bodies revealed that their number of lipofuscin granules, extracellular space pockets containing or not debris, elongated mitochondria, as well as dilated ER and Golgi apparatus cisternae did not differ significantly between experimental groups (Table 2 and Supp. Fig. 2 for representative examples of these organelles). Nevertheless, the number of endosomes per IBA1-positive cell body was significantly reduced in MPTP monkeys compared with control ones (4.250 ± 0.4027 in MPTP *versus* 5.527 ± 0.3972 in control animals, $p = 0.0466$) (Fig. 4H), suggesting a reduced phagocytic activity. This number of endosomes per IBA1-positive cell body was not normalized by L-Dopa treatment (3.611 ± 0.4482 in MPTP + L-Dopa animals, $p = 0.5904$) (Fig. 4H). The number of primary lysosomes per IBA1-positive cell body nevertheless increased in MPTP monkeys treated with L-Dopa compared to untreated MPTP monkeys (0.4815 ± 0.1877 in MPTP + L-Dopa *versus* 0.07895 ± 0.0433 in MPTP animals, $p = 0.0171$) (Fig. 4I), which may suggest a compensatory mechanism. Lastly, the numbers of secondary or tertiary lysosomes per IBA1-positive cell body were not significantly different between groups (Fig. 4J,K). Together, these findings point toward an impairment of the phagolysosomal system in microglia during PD pathophysiology that is partially reversed by L-Dopa treatment.

Lastly, to provide insights into this change in microglial phagolysosomal activity on a molecular level, we performed a double immunostaining against IBA1 and CD68, a glycoprotein associated with endosomes and lysosomes (Fig. 5). Observations were made in the sensorimotor region of the putamen by confocal microscopy. By counting the number of CD68 puncta per IBA1-positive cell, when comparing total cells or cell bodies and process arborizations separately, we did not detect significant differences between the control and MPTP monkey groups (Fig. 5J-L). Nevertheless, the density of CD68 puncta per IBA1-positive cell was reduced in MPTP monkeys treated with L-Dopa compared with non-treated MPTP animals (total cell: 18.00 ± 0.6373 in MPTP *vs* 12.17 ± 0.6774 in MPTP + L-Dopa, $p < 0.0001$). Similarly, the density of CD68 puncta per IBA1-positive cells was reduced in MPTP monkeys treated with L-Dopa compared with non-treated MPTP animals when considering cell bodies (4.013 ± 0.1657 in MPTP *versus* 3.008 ± 0.1673 in L-Dopa treated animals, $p < 0.0001$) and arborizations (13.99 ± 0.5837 in MPTP *versus* 9.111 ± 0.5896 in L-Dopa treated animals, $p < 0.0001$) separately (Fig. 5J-L). To confirm that CD68 expression in striatal microglia is, as expected from the literature, associated with their phagolysosomal system, in which endosomes fuse with lysosomal vesicles to degrade cellular constituents (Eskelinen and Saftig, 2009), we lastly performed an immunocytochemical electron microscopy against CD68. Our ultrastructural observations confirmed that CD68 localizes to endosomes, as well as secondary lysosomes and tertiary residual debris, with some staining observed on the plasma membrane, in microglia from the sensorimotor putamen (Fig. 5M,N). These results together indicate that microglial degradation activity is compromised during PD pathophysiology and that this disruption partially prevails in the context of LID (Fig. 6).

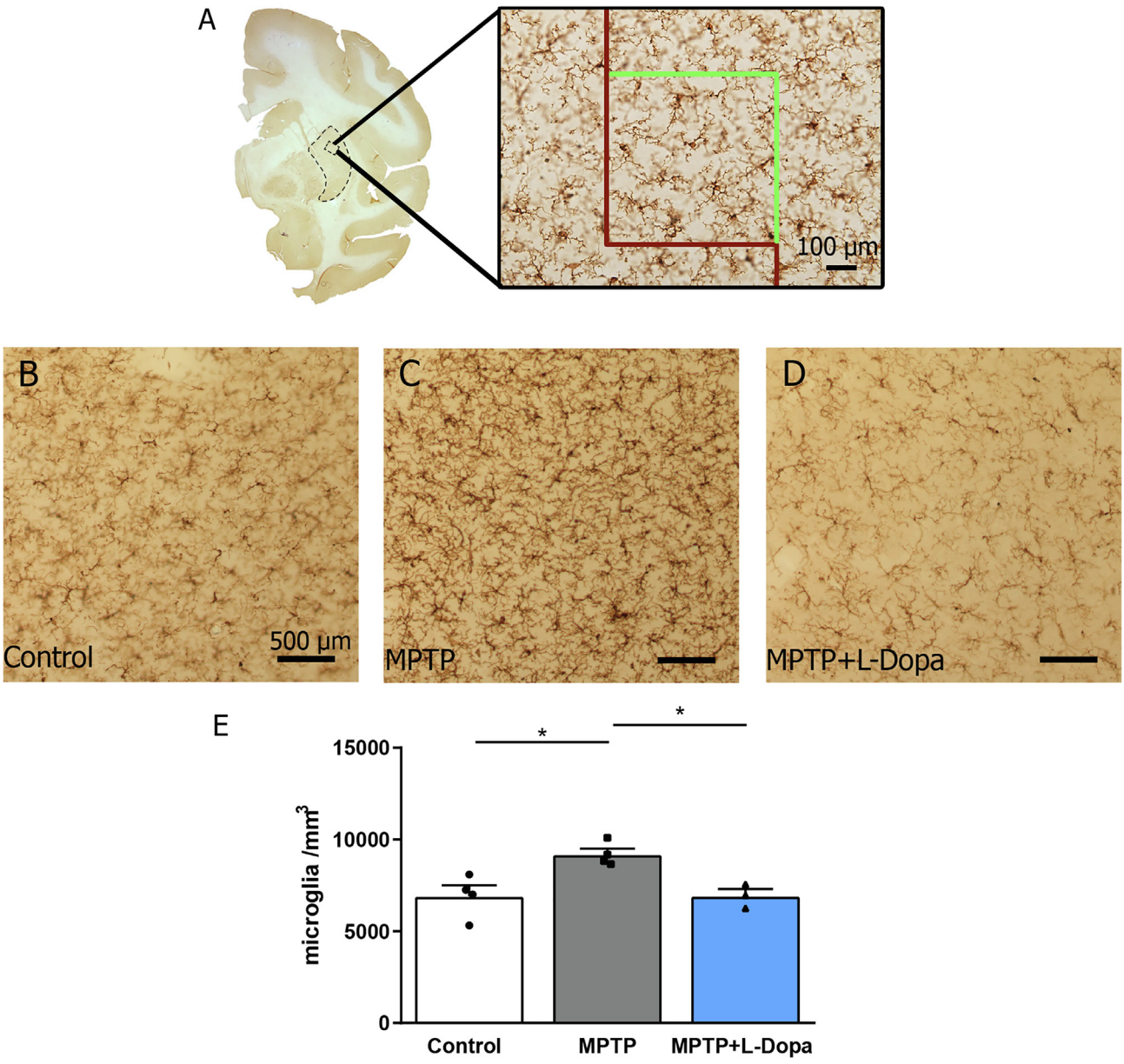

Fig. 2. Effects of MPTP and L-Dopa treatment on microglial density in the striatum of macaque monkeys. A: Example of a counting frame used for the stereological assessment of microglial density in the sensorimotor putamen. B-D: Representative images of IBA1-positive cells in (B) a control monkey, (C) a MPTP-intoxicated monkey, and (D) a MPTP monkey treated with L-Dopa. E: The histogram shows the number of IBA1-positive cells per mm^3 in the sensorimotor putamen of the three experimental groups. Statistically significant differences were obtained between control and MPTP monkeys, as well as between MPTP and MPTP with L-Dopa animals. Data shown are expressed as means ± S.E.M. * $p < 0.05$, by using one-way ANOVA followed by a Bonferroni *post-hoc* test. Scale bars: 100 µm (A) and 500 µm (B-D).

4. Discussion

The present study characterized the changes in IBA1-positive cell density, morphology, and phagocytosis during PD pathophysiology, including chronic L-Dopa treatment causing LID, using a MPTP monkey model that best recapitulates motor symptoms of the disease. In particular, we examined the sensorimotor territory of the putamen, considering that DA denervation is most severe in this striatal region of MPTP monkeys (Gagnon et al., 2016). Our results using IBA1 staining revealed that striatal microglia become more abundant and shift their morphological phenotype towards enlarged cell body with more extended process arborization compared with control animals. These changes in microglia previously associated with a "mild activation" in other contexts (Kanaan et al., 2008; Hinwood et al., 2013; Tynan et al., 2013; Hui et al., 2018) were normalized to control values upon L-Dopa treatment. A decreased number of endosomes inside striatal IBA1-positive cell bodies in the MPTP group that was not reversed by L-Dopa treatment was nevertheless measured at the ultrastructural level. Moreover, primary lysosomes increased in number in the IBA1-positive cell bodies from the MPTP group treated with L-Dopa while no differences were observed for secondary and tertiary lysosomes. In addition, IBA1-positive cell expression of CD68, associated with phagolysosomal activity, was not changed with MPTP but significantly decreased with L-Dopa, when measured by confocal microscopy, indicating a partial microglial phagolysosomal dysfunction in the L-Dopa-treated group experiencing LID. To our knowledge, this is the first report on the effects of L-Dopa on microglial phenotype in the striatum of MPTP monkeys. Overall, these results support the importance of studying the roles of microglia in PD pathophysiology, beyond the acute stage of DA denervation and during chronic L-Dopa treatment when LID are

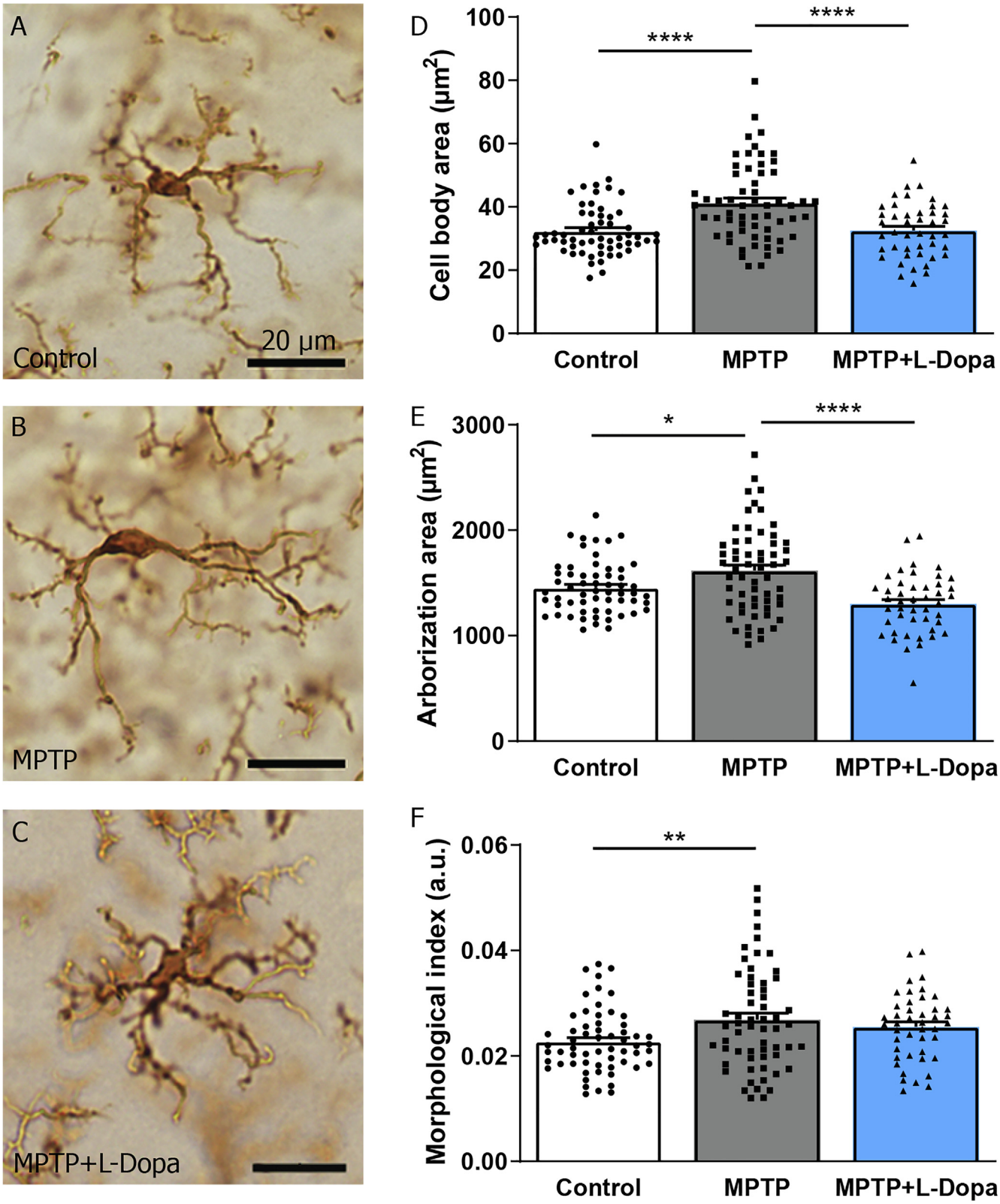

Fig. 3. Effects of MPTP and L-Dopa treatment on microglial cell body and arborization area, as well as morphological index in the striatum of macaque monkeys. A-C: High magnification photomicrographs showing IBA1-positive cells in the sensorimotor putamen of (A) control, (B) MPTP and (C) MPTP + L-Dopa monkeys. D-F: Histograms showing the quantification of microglial (D) cell body area (μm^2), (E) arborization area (μm^2), and (F) morphological index (arbitrary units; a.u.) in the three experimental groups. Data shown are expressed as means ± S.E.M. $^{*}p < 0.05$, $^{**}p < 0.01$, $^{****}p < 0.0001$, by one-way ANOVA followed by a Bonferroni *post-hoc* test. Scale bars: 20 µm.

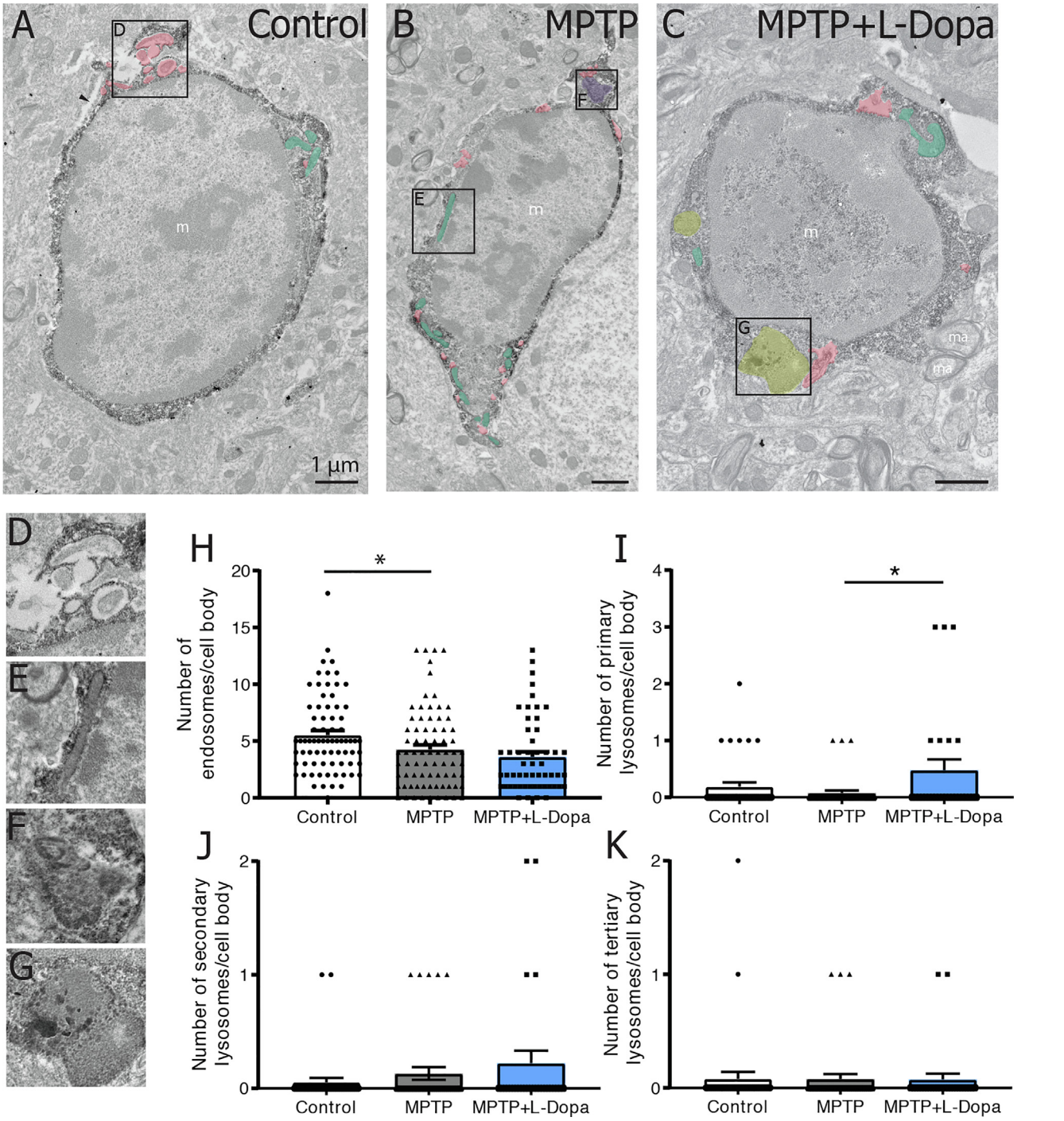

Fig. 4. Effects of MPTP and L-Dopa treatment on microglial ultrastructure in the striatum of macaque monkeys. A-C: Representative images of IBA1-positive cell bodies in (A) control, (B) MPTP and (C) MPTP-treated with L-Dopa monkeys. D-G: Representative higher magnification images of (D) endosome, (E) elongated mitochondrion, (F) lipofuscin granule, and (g) primary lysosome. H-I: Histograms showing the number of (H) endosomes, (I) primary lysosomes, (J) secondary lysosomes, and (K) tertiary lysosomes per microglial cell body in the three experimental groups. Statistically significant differences were obtained between control and MPTP monkeys, as well as between MPTP and MPTP with L-Dopa animals. Data shown are expressed as means ± S.E.M. * $p < 0.05$, by using one-way ANOVA followed by a Bonferroni *post-hoc* test. Pink: endosomes, yellow: primary lysosomes, purple: lipofuscin granules, and green: mitochondria. Black arrows: extracellular space pockets, m: microglia, ma: myelinated axons. Scale bars: 1 µm. (For interpretation of the references to colour in this figure legend, the reader is referred to the web version of this article.)

experienced.

In our MPTP monkey model, we measured by stereology an increased number of IBA1-positive cells in the sensorimotor region of the putamen. In addition to yolk-sac derived resident microglia, a small number of bone marrow-derived monocytes can infiltrate the brain and differentiate into microglia-like cells expressing IBA1. This raised the intriguing possibility that peripheral myeloid cells could at least partially explain the measured increase in IBA1-positive cells density. We observed in the striatum of our MPTP monkey model an increased proportion of IBA1-positive cells that were immunonegative for TMEM119, which is considered a microglia-specific marker (Bennett et al., 2016), thus supporting this hypothesis. The density of IBA1-

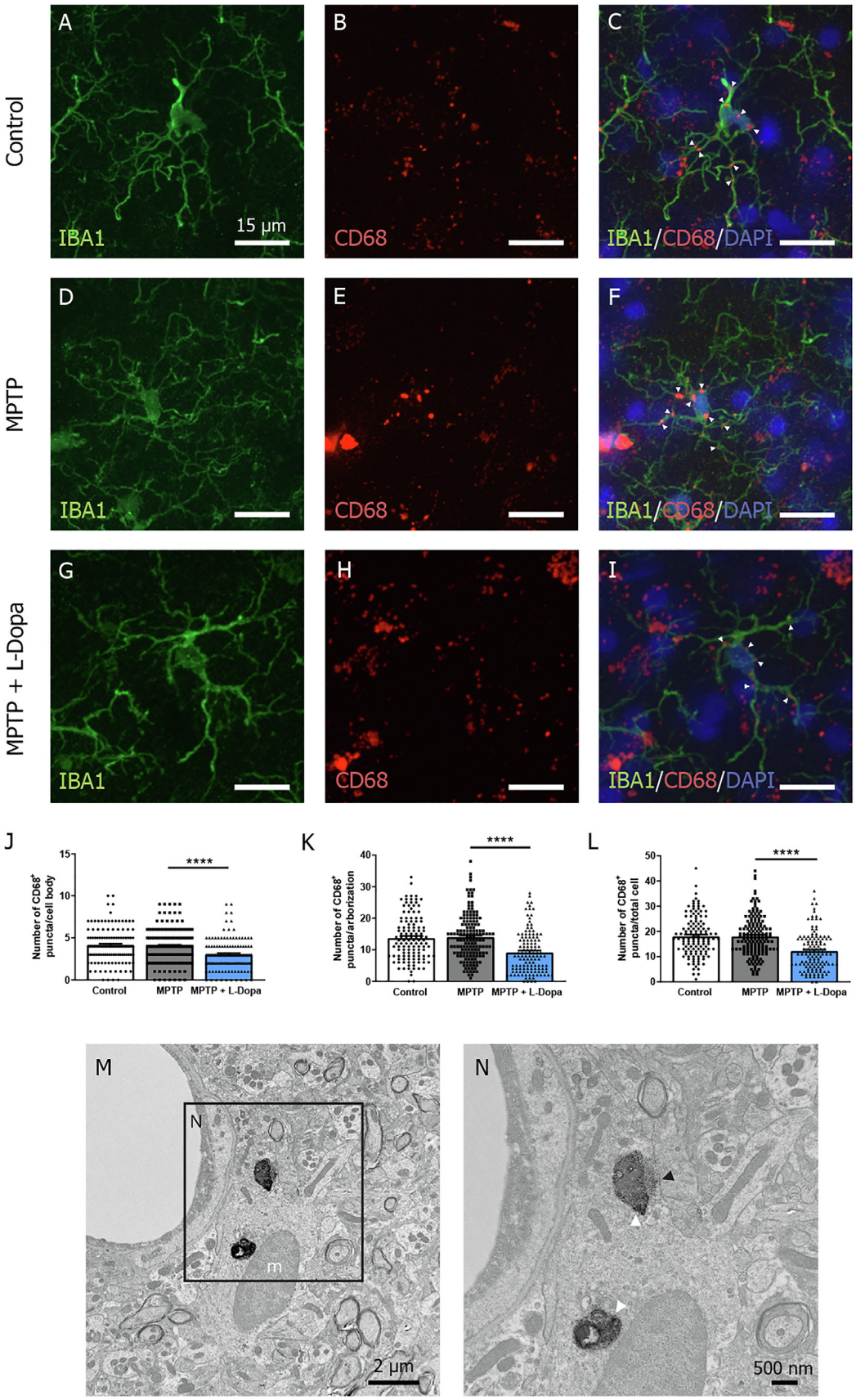

Fig. 5. Effects of MPTP and L-Dopa treatment on microglial phagolysosomal activity in the striatum of macaque monkeys. A-I: representative confocal images showing CD68-positive puncta in IBA1-positive cells: (A, D, G) IBA1-positive cell, (B, E, H) CD68-positive puncta, and (C, F, I) merged imaged, from the sensorimotor putamen region of the three experimental groups. J-L: Histogram showing the number of CD68-positive puncta per IBA1-positive (J) cell body, (K) process arborization and (L) total cell. M−N: Localization of CD68-positive staining in microglia at the ultrastructural level. White arrowheads: endolysosomal compartment, black arrowhead: plasma membrane. Data are represented as means ± S.E.M. **** $p < 0.0001$, by using one-way ANOVA followed by a Bonferroni *post-hoc* test. Scale bar: 15 µm.

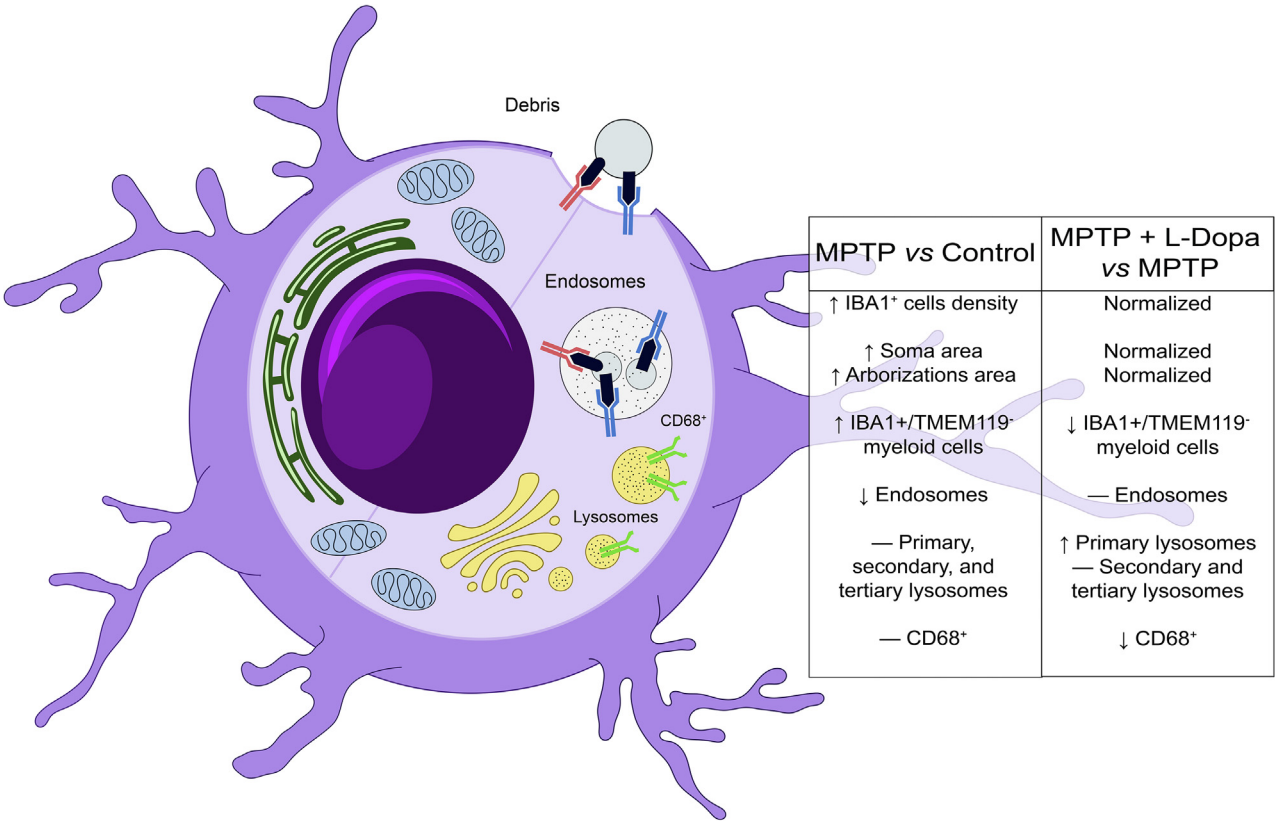

Fig. 6. Schematic representation of the main findings of this study.

positive/TMEM119-negative cells was further reduced in the MPTP animals treated with L-Dopa, reaching control values. Infiltration in the MPTP animals could result from an increase in blood brain barrier (BBB) permeability over the course of pathology, considering that BBB leakage was previously reported in the SN and striatum of a MPTP mouse model using fluoresceinisothiocyanate-labeled albumin (FITC-LA) (Zhao et al., 2007). Similar to our findings with IBA1, previous studies have reported increased expression of major histocompatibility complex (MHC) class II-positive cells in human PD brains, across the SN, putamen and hippocampus, only to name a few regions (Imamura et al., 2003), or human leukocyte antigen (HLA)-DR positive cells in the SN *pars compacta* of MPTP cynomolgus monkeys (Barcia et al., 2004). MHC class II and HLA-DR are expressed by microglia and other populations of myeloid cells (McGeer et al., 1988; Perry et al., 2010). While MHC class II is classically considered to be a marker of antigen presentation (Weenink and Gautam, 1997), it is expressed by reactive microglia and associated with other neurodegenerative conditions such as Alzheimer's disease (Hopperton et al., 2018).

In addition to their changes in density, microglia can transform from a ramified to an amoeboid morphology characterized by shorter processes and a bigger cell body (Davis et al., 2017). These morphological changes together define a reactive or "activated" microglial phenotype (Nayak et al., 2014; Tay et al., 2017). Amoeboid microglia are generally considered to be highly phagocytic (Davis et al., 2017). Here, we observed instead a shift towards hyper-ramified cells, which are considered to be "mildly activated" (Walker et al., 2014), in the putamen of MPTP monkeys. Our results are in accordance with the study of Hurley and colleagues in which MHC class II-positive cells were compared between control and MPTP macaque monkeys. In the striatum, microglia were mainly taking a ramified morphology. By contrast, in the same study, MHC class II-positive microglia of the SN, nigrostriatal tract and globus pallidus displayed heterogeneous morphologies: either ramified, amoeboid or multinucleated (Hurley et al., 2003). Of note, this hyper-ramified morphological phenotype observed in PD pathology might be exclusive to primates including humans (Imamura et al., 2003), since amoeboid microglia were seen most of the time in the striatum and SN of MPTP mice (Kurkowska-Jastrzebska et al., 1999; Wu et al., 2002). These apparent differences between studies could be attributed to differences in species (Hurley et al., 2003). Indeed, distinctions between rodent and human microglia were described, pertaining to their proliferative capacity, transforming growth factor (TGF)β signaling response, as well as expression of TNFγ receptors and histocompatibility complexes (Kreutzberg, 1996; Grow et al., 2016).

The normalization of both microglial numeral and morphological alterations by L-Dopa treatment might indicate a partial rescue of their physiological functions. In fact, microglia express DA receptors, with some difference regarding the exact subtypes between studies, in both mouse and human microglial cells *in vitro* (Färber et al., 2005; Mastroeni et al., 2009). DA influences microglial migration and induces potassium current changes in rodent brain slices (Färber et al., 2005). In the latter study, a reduction of microglial nitric oxide release was also observed with DA treatment after a challenge with LPS. However, DA did not modulate microglial release of the pro-inflammatory cytokines TNFα and IL-6 (Färber et al., 2005). Additionally, L-Dopa therapy was shown to reduce the oxidative stress measured in peripheral blood mononuclear cells from PD patients (Prigione et al., 2006). Nevertheless, several studies have reported increased levels of the inflammatory markers cyclooxygenase-2 (COX2) and inducible nitric oxide synthase (iNOS) in the striatum of 6-OHDA-lesioned rats treated with L-Dopa and experiencing LID (Del-Bel et al., 2016; Carta et al., 2017). High doses of L-Dopa were also shown to produce oxidative stress *in vivo*, leading to neuronal death by apoptosis (Jin et al., 2010; Sabens et al., 2011). However, it remains unclear if microglia are involved or not in mediating these outcomes (Peterson and Flood, 2012). In agreement with our observation, both high (25 mg/kg) and low (6 mg/kg) doses of chronic L-Dopa treatment in 6-OHDA-lesioned rats

resulted in abnormal involuntary movements but without any detectable morphological aberration in CD68 (ED-1) positive cells within the striatum (Lindgren et al., 2007).

The expression of CD68, also known as macrosialin in mice, in IBA1-positive cells was unchanged in our MPTP-intoxicated monkeys. However, their treatment with L-Dopa significantly reduced IBA1/CD68 colocalization, both in cell bodies and ramifications, even below control levels. In a similar study, Lindgren et al. (2007) observed minimal CD68 (ED-1) immunoreactivity in L-Dopa treated 6-OHDA-lesioned rats with abnormal involuntary movements, although stereological assessment was not performed (Lindgren et al., 2007). While the interpretation of this finding is unclear, the CD68 protein is upregulated in phagocytic cells where it localizes to secondary and tertiary lysosomal membranes, as well as endosomes (Zotova et al., 2013), and can also transit to the plasma membrane (Chistiakov et al., 2017), as confirmed by our ultrastructural observations in striatal microglia. Contrary to our findings in the putamen of MPTP monkeys, it was previously shown in the SN of *post-mortem* PD patients that microglial CD68 expression is increased (Croisier et al., 2005; Doorn et al., 2014). Theodore and colleagues associated this CD68 increase in the SN to early neurodegeneration in a PD mouse model overexpressing human α-synuclein (Theodore et al., 2008). Another group correlated the CD68 increase to DA neuronal death in the SN of rats expressing human α-synuclein (Sanchez-Guajardo et al., 2010). These results together suggest that microglia undergo region-specific changes in phagolysosomal activity over the course of PD pathophysiology. In accordance with previous data regarding the outcome of neuronal activity and the neuromodulator DA on microglial properties (Biber et al., 2007), including phagocytosis, L-Dopa treatment could keep microglia in a "homeostatic" or surveillant state (Fan et al., 2018). While the MPTP monkeys receiving L-Dopa suffered from LID, and might display exacerbated remodeling of serotoninergic axon projections in the putamen as previously shown in MPTP monkeys (Gagnon et al., 2016), whether the observed phagolysosomal changes in microglia contribute or not to LID still remains elusive.

Our ultrastructural analyses of IBA1-positive cell bodies in the sensorimotor region of the putamen of MPTP monkeys revealed no difference in their prevalence of dilated ER/Golgi organelles, elongated mitochondria, lipofuscin granules, associated extracellular space (with or without debris), and synaptic contacts, suggesting that microglial functions are generally preserved in the different groups. Nevertheless, a significant decrease in the number of endosomes per microglial cell body was observed in the MPTP monkeys, and this was not restored by L-Dopa. This may be an indication of an accumulated phagocytic cargo which overwhelms and impairs microglial phagocytic clearance (Dal Ben et al., 2019; Tremblay et al., 2019). An impaired microglial phagocytosis was previously described in aging and several other contexts of neurodegeneration, supporting the view that microglial dysfunction (in addition to "mild activation") might contribute to pathology (Streit, 2002; Tremblay et al., 2019). Further, the observed alteration in phagocytosis was accompanied by an increase in the number of primary lysosomes in MPTP monkeys receiving L-Dopa, without changes in secondary or tertiary lysosomes. The increased prevalence of primary lysosomes could reflect a compensatory mechanism at play to restore aggravated impaired microglial phagocytic activity (Awogbindin et al., 2020). During PD and its treatment with L-Dopa, α-synuclein progressively accumulates (Xu and Chan, 2015; Herrera et al., 2017). Consequently, traditional phagocytic clearance becomes impaired, paving way for non-conventional clearance mechanisms such as Toll-like receptor 4 (TLR4)-mediated clearance with attendant NF-κB-dependent pro-inflammatory responses (Stefanova et al., 2011). Indeed, Choi et al. (Choi et al., 2020) demonstrated that the uptake of overwhelming levels of extracellular and neuron-released α-synuclein by microglia is not mediated by endosome-dependent phagocytic or endocytic process. Rather, accumulated α-synuclein was shown to be engulfed by a lysosome-associated process that involves a TL4-mediated NF-κB-dependent upregulation of the autophagy receptor marker p62/SQSTM1 (Choi et al., 2020). In the study, pharmacological treatment of microglia with inhibitors of lysosomal acidification, Bafilomycin A1/ Chloroquine, or treatment of p62- or TLR4-defficient microglial cells with α-synuclein aborted the clearance of human α-synuclein, thereby exposing DA neurons to further degeneration (Choi et al., 2020). Whether the autophagolysosomal dysfunction observed during LID in the current study is associated with the described microglial "synucleinphagy" in human PD patients awaits detailed investigation.

A limitation of the present study is that a time course of microglial changes after MPTP in monkeys was not assessed for a better comparison with other studies. Hence the time after the lesion, the extent of the lesion, the sex of the animals and if they are gonadectomised all affect microglia. In 6-OHDA rats as a model of PD, IBA1 immunofluorescence measures in the SN showed an early mild/moderate increase, (1 day after 6-OHDA lesion) followed by a mild increase (days 2–7 post 6-OHDA) and then a moderate increase (14 days post lesion) in ovariectomized females whereas in intact males and females the increase was mild early on (days 1–2) and unchanged afterwards (days 7–14) (Siani et al., 2017). By contrast, an extensive MPTP lesion in male mice was associated with elevated IBA1 protein levels in the striatum measured by Western blots both 3 and 7 days after MPTP (Takagi et al., 2007).

5. Conclusion

Our findings indicate that MPTP administration to *cynomolgus* monkeys alters microglial density, morphology and phagolysosomal activity in the sensorimotor functional territory of the putamen, which are partially normalized by L-Dopa treatment. In particular, MPTP monkeys showed an increased density of IBA1-positive cells that was associated with a small, although significant increase in peripheral myeloid cells (IBA1-positive/TMEM119-negative). Microglia from MPTP animals also displayed a hyper-ramified morphology associated with a "mild-activation" that was normalized following L-Dopa exposure. Microglial phagolysosomal activity was further altered in MPTP monkeys, as shown by their decreased number of endosomes measured by transmission electron microscopy. This alteration was partially restored by L-Dopa treatment, which increased microglial numbers of primary but not of secondary and tertiary lysosomes, and reduced CD68 positive puncta in IBA1-positive cells. Our study highlights the importance of investigating microglial functional implication during PD pathophysiology, including LID. Comparing the roles exerted by microglia in MPTP monkeys with and without LID could also help to understand how these immune cells are specifically involved in this deleterious process and probably predict a target for future therapeutics.

Declaration of Competing Interest

The authors declare that they have no known competing financial interests or personal relationships that could have appeared to influence the work reported in this paper.

Acknowledgements

We thank Julie-Christine Lévesque at the Bioimaging platform of the *Infectious Disease Research Centre*, funded by the Canadian Foundation Innovation (CFI). We are also grateful to Laurent Grégoire, Marie-Josée Wallman, Micaël Carrier, and Nathalie Vernoux for their contribution to the study, as well as Laura Civiero for revising the manuscript. C.L. was recipient of a master training award from Fonds de Recherche du Québec – Santé (FRQS), an excellence award from Département de médecine moléculaire of Université Laval, and an excellence award Didier-Mouginot from Fondation du CHU de Québec. M.K.S.P. is

supported by a scholarship from Université Laval and an excellence award from Fondation du CHU de Québec, as well as master and doctoral training awards from Canadian Institutes of Health Research (CIHR) and FRQS. M. Bordeleau is recipient a doctoral training award from FRQS. K.P. is supported by an excellence award from Fondation du CHU de Québec, as well as from Centre thématique de recherche en neurosciences and from Fondation Famille-Choquette. IOA is supported by an International Brain Research Organization African Regional Committee (IBRO-ARC) 2019 Fellowship at Université Laval, Québec, QC, Canada. F.G.I. is supported by a scholarship from the Mexican Council of Science and Technology (CONACYT). The study was funded by an operating grant from CIHR (#341846) awarded to T.D.P., L.C., M.P. and M.E.T. M.E.T. held a Tier II Canada Research Chair in *Neuroimmune plasticity in health and therapy* (2017-20) and now holds a Tier II Canada Research Chair in *Neurobiology of Aging and Cognition* (2020-25).

Data sharing statement

The data that support the findings of this study are available from the corresponding authors, TDP and MET, upon reasonable request.

Appendix A. Supplementary data

Supplementary data to this article can be found online at https://doi.org/10.1016/j.bbi.2020.07.044.

References

Ahlskog, J.E., Muenter, M.D., 2001. Frequency of levodopa-related dyskinesias and motor fluctuations as estimated from the cumulative literature. Mov Disord Off J Mov Disord Soc 16, 448–458.

Awogbindin, I.O., Ishola, I.O., St-Pierre, M.-K., Carrier, M., Savage, J.C., Di Paolo, T., Tremblay, M.-È., 2020. Remodeling microglia to a protective phenotype in Parkinson's disease? Neurosci Lett 735, 135164.

Barnum, C.J., Eskow, K.L., Dupre, K., Blandino, P., Deak, T., Bishop, C., 2008. Exogenous corticosterone reduces L-DOPA-induced dyskinesia in the hemi-parkinsonian rat: role for interleukin-1beta. Neuroscience 156, 30–41.

Bennett, M.L., Bennett, F.C., Liddelow, S.A., Ajami, B., Zamanian, J.L., Fernhoff, N.B., Mulinyawe, S.B., Bohlen, C.J., Adil, A., Tucker, A., Weissman, I.L., Chang, E.F., Li, G., Grant, G.A., Hayden Gephart, M.G., Barres, B.A., 2016. New tools for studying microglia in the mouse and human CNS. Proc Natl Acad Sci U S A 113, E1738–E1746.

Biber, K., Neumann, H., Inoue, K., Boddeke, H.W.G.M., 2007. Neuronal "On" and "Off" signals control microglia. Trends Neurosci 30, 596–602.

Carta, A.R., Mulas, G., Bortolanza, M., Duarte, T., Pillai, E., Fisone, G., Vozari, R.R., Del-Bel, E., 2017. l-DOPA-induced dyskinesia and neuroinflammation: do microglia and astrocytes play a role? Eur J Neurosci 45, 73–91.

Chaudhuri, K.R., Jenner, P., Antonini, A., 2019. Should there be less emphasis on levodopa-induced dyskinesia in Parkinson's disease? Mov Disord Off J Mov Disord Soc 34, 816–819.

Chistiakov, D.A., Killingsworth, M.C., Myasoedova, V.A., Orekhov, A.N., Bobryshev, Y.V., 2017. CD68/macrosialin: not just a histochemical marker. Lab Invest 97, 4–13.

Choi I, Zhang Y, Seegobin SP, Pruvost M, Wang Q, Purtell K, Zhang B, Yue Z. 2020. Microglia clear neuron-released α-synuclein via selective autophagy and prevent neurodegeneration. Nat Commun [Internet] 11. Available from: https://www.ncbi.nlm.nih.gov/pmc/articles/PMC7069981/.

Choi, Y.R., Kang, S.-J., Kim, J.-M., Lee, S.-J., Jou, I., Joe, E.-H., Park, S.M., 2015. FcγRIIB mediates the inhibitory effect of aggregated α-synuclein on microglial phagocytosis. Neurobiol Dis 83, 90–99.

Croisier, E., Moran, L.B., Dexter, D.T., Pearce, R.K., Graeber, M.B., 2005. Microglial inflammation in the parkinsonian substantia nigra: relationship to alpha-synuclein deposition. J Neuroinflammation 2, 14.

Dal Ben M, Bongiovanni R, Tuniz S, Fioriti E, Tiribelli C, Moretti R, Gazzin S. 2019. Earliest Mechanisms of Dopaminergic Neurons Sufferance in a Novel Slow Progressing Ex Vivo Model of Parkinson Disease in Rat Organotypic Cultures of Substantia Nigra. Int J Mol Sci [Internet] 20. Available from: https://www.ncbi.nlm.nih.gov/pmc/articles/PMC6539377/.

Davis BM, Salinas-Navarro M, Cordeiro MF, Moons L, De Groef L. 2017. Characterizing microglia activation: a spatial statistics approach to maximize information extraction. Sci Rep [Internet] 7. Available from: https://www.ncbi.nlm.nih.gov/pmc/articles/PMC5431479/.

Del-Bel, E., Bortolanza, M., Dos-Santos-Pereira, M., Bariotto, K., Raisman-Vozari, R., 2016. l-DOPA-induced dyskinesia in Parkinson's disease: Are neuroinflammation and astrocytes key elements? Synap N Y N 70, 479–500.

Doorn KJ, Moors T, Drukarch B, van de Berg WD, Lucassen PJ, van Dam A-M. 2014. Microglial phenotypes and toll-like receptor 2 in the substantia nigra and hippocampus of incidental Lewy body disease cases and Parkinson's disease patients. Acta Neuropathol Commun [Internet] 2. Available from: https://www.ncbi.nlm.nih.gov/pmc/articles/PMC4224021/.

Durif, F., Debilly, B., Galitzky, M., Morand, D., Viallet, F., Borg, M., Thobois, S., Broussolle, E., Rascol, O., 2004. Clozapine improves dyskinesias in Parkinson disease: a double-blind, placebo-controlled study. Neurology 62, 381–388.

El Hajj, H., Savage, J.C., Bisht, K., Parent, M., Vallières, L., Rivest, S., Tremblay, M.-È., 2019. Ultrastructural evidence of microglial heterogeneity in Alzheimer's disease amyloid pathology. J Neuroinflammation 16, 87.

Eskelinen, E.-L., Saftig, P., 2009. Autophagy: a lysosomal degradation pathway with a central role in health and disease. Biochim Biophys Acta 1793, 664–673.

Fabbrini G, Brotchie JM, Grandas F, Nomoto M, Goetz CG. 2007. Levodopa-induced dyskinesias. Mov Disord Off J Mov Disord Soc 22:1379–1389; quiz 1523.

Fahn S, Oakes D, Shoulson I, Kieburtz K, Rudolph A, Lang A, Olanow CW, Tanner C, Marek K, Parkinson Study Group. 2004. Levodopa and the progression of Parkinson's disease. N Engl J Med 351:2498–2508.

Fan Y, Chen Z, Pathak JL, Carneiro AMD, Chung CY. 2018. Differential Regulation of Adhesion and Phagocytosis of Resting and Activated Microglia by Dopamine. Front Cell Neurosci [Internet] 12. Available from: https://www.ncbi.nlm.nih.gov/pmc/articles/PMC6141656/.

Färber, K., Pannasch, U., Kettenmann, H., 2005. Dopamine and noradrenaline control distinct functions in rodent microglial cells. Mol Cell Neurosci 29, 128–138.

Fasano, M., Giraudo, S., Coha, S., Bergamasco, B., Lopiano, L., 2003. Residual substantia nigra neuromelanin in Parkinson's disease is cross-linked to alpha-synuclein. Neurochem Int 42, 603–606.

Gagnon, D., Gregoire, L., Di Paolo, T., Parent, M., 2016. Serotonin hyperinnervation of the striatum with high synaptic incidence in parkinsonian monkeys. Brain Struct Funct 221, 3675–3691.

González Ibanez F, Picard K, Bordelau M, Sharma K, Bisht K, Tremblay M-È. 2019. Immunofluorescence Staining Using IBA1 and TMEM119 for Microglial Density, Morphology and Peripheral Myeloid Cell Infiltration Analysis in Mouse Brain. J Vis Exp JoVE.

Grow, D.A., McCarrey, J.R., Navara, C.S., 2016. Advantages of nonhuman primates as preclinical models for evaluating stem cell-based therapies for Parkinson's disease. Stem Cell Res 17, 352–366.

Hadj Tahar, A., Grégoire, L., Darré, A., Bélanger, N., Meltzer, L., Bédard, P.J., 2004. Effect of a selective glutamate antagonist on L-dopa-induced dyskinesias in drug-naive parkinsonian monkeys. Neurobiol Dis 15, 171–176.

Haka, A.S., Barbosa-Lorenzi, V.C., Lee, H.J., Falcone, D.J., Hudis, C.A., Dannenberg, A.J., Maxfield, F.R., 2016. Exocytosis of macrophage lysosomes leads to digestion of apoptotic adipocytes and foam cell formation. J Lipid Res 57, 980–992.

Hauser, R.A., Pahwa, R., Tanner, C.M., Oertel, W., Isaacson, S.H., Johnson, R., Felt, L., Stempien, M.J., 2017. ADS-5102 (Amantadine) Extended-Release Capsules for Levodopa-Induced Dyskinesia in Parkinson's Disease (EASE LID 2 Study): Interim Results of an Open-Label Safety Study. J Park Dis 7, 511–522.

Herrera, A., Muñoz, P., Steinbusch, H.W.M., Segura-Aguilar, J., 2017. Are Dopamine Oxidation Metabolites Involved in the Loss of Dopaminergic Neurons in the Nigrostriatal System in Parkinson's Disease? ACS Chem Neurosci 8, 702–711.

Hinwood, M., Tynan, R.J., Charnley, J.L., Beynon, S.B., Day, T.A., Walker, F.R., 2013. Chronic stress induced remodeling of the prefrontal cortex: structural re-organization of microglia and the inhibitory effect of minocycline. Cereb Cortex N Y N 1991 (23), 1784–1797.

Hong, J.Y., Oh, J.S., Lee, I., Sunwoo, M.K., Ham, J.H., Lee, J.E., Sohn, Y.H., Kim, J.S., Lee, P.H., 2014. Presynaptic dopamine depletion predicts levodopa-induced dyskinesia in de novo Parkinson disease. Neurology 82, 1597–1604.

Hopperton, K.E., Mohammad, D., Trépanier, M.O., Giuliano, V., Bazinet, R.P., 2018. Markers of microglia in post-mortem brain samples from patients with Alzheimer's disease: a systematic review. Mol Psychiatry 23, 177–198.

Hubsher, G., Haider, M., Okun, M.S., 2012. Amantadine: the journey from fighting flu to treating Parkinson disease. Neurology 78, 1096–1099.

Hui, C.W., St-Pierre, M.-K., Detuncq, J., Aumailley, L., Dubois, M.-J., Couture, V., Skuk, D., Marette, A., Tremblay, J.P., Lebel, M., Tremblay, M.-È., 2018. Nonfunctional mutant Wrn protein leads to neurological deficits, neuronal stress, microglial alteration, and immune imbalance in a mouse model of Werner syndrome. Brain Behav Immun 73, 450–469.

Huot, P., Johnston, T.H., Koprich, J.B., Fox, S.H., Brotchie, J.M., 2013. The pharmacology of L-DOPA-induced dyskinesia in Parkinson's disease. Pharmacol Rev 65, 171–222.

Hurley, S.D., O'Banion, M.K., Song, D.D., Arana, F.S., Olschowka, J.A., Haber, S.N., 2003. Microglial response is poorly correlated with neurodegeneration following chronic, low-dose MPTP administration in monkeys. Exp Neurol 184, 659–668.

Imamura, K., Hishikawa, N., Sawada, M., Nagatsu, T., Yoshida, M., Hashizume, Y., 2003. Distribution of major histocompatibility complex class II-positive microglia and cytokine profile of Parkinson's disease brains. Acta Neuropathol (Berl) 106, 518–526.

Jankovic, J., 2008. Parkinson's disease: clinical features and diagnosis. J Neurol Neurosurg Psychiatry 79, 368–376.

Jin, C.M., Yang, Y.J., Huang, H.S., Kai, M., Lee, M.K., 2010. Mechanisms of L-DOPA-induced cytotoxicity in rat adrenal pheochromocytoma cells: implication of oxidative stress-related kinases and cyclic AMP. Neuroscience 170, 390–398.

Julien, C., Berthiaume, L., Hadj-Tahar, A., Rajput, A.H., Bédard, P.J., Di Paolo, T., Julien, P., Calon, F., 2006. Postmortem brain fatty acid profile of levodopa-treated Parkinson disease patients and parkinsonian monkeys. Neurochem Int 48, 404–414.

Kanaan, N.M., Kordower, J.H., Collier, T.J., 2008. Age and region-specific responses of microglia, but not astrocytes, suggest a role in selective vulnerability of dopamine neurons after 1-methyl-4-phenyl-1,2,3,6-tetrahydropyridine exposure in monkeys. Glia 56, 1199–1214.

Kim, J.-H., Lee, H.-W., Hwang, J., Kim, J., Lee, M.-J., Han, H.-S., Lee, W.-H., Suk, K., 2012. Microglia-inhibiting activity of Parkinson's disease drug amantadine.

Neurobiol Aging 33, 2145–2159.
Kostrzewa, R.M., Kostrzewa, J.P., Brus, R., 2002. Neuroprotective and neurotoxic roles of levodopa (L-DOPA) in neurodegenerative disorders relating to Parkinson's disease. Amino Acids 23, 57–63.
Kreutzberg, G.W., 1996. Microglia: a sensor for pathological events in the CNS. Trends Neurosci 19, 312–318.
Kurkowska-Jastrzebska, I., Wrońska, A., Kohutnicka, M., Członkowski, A., Członkowska, A., 1999. The inflammatory reaction following 1-methyl-4-phenyl-1,2,3, 6-tetrahydropyridine intoxication in mouse. Exp Neurol 156, 50–61.
Lebouvier T, Chaumette T, Paillusson S, Duyckaerts C, Bruley des Varannes S, Neunlist M, Derkinderen P. 2009. The second brain and Parkinson's disease. Eur J Neurosci 30:735–741.
Lehéricy, S., Benali, H., Van de Moortele, P.-F., Pélégrini-Issac, M., Waechter, T., Ugurbil, K., Doyon, J., 2005. Distinct basal ganglia territories are engaged in early and advanced motor sequence learning. Proc Natl Acad Sci U S A 102, 12566–12571.
Lindgren, H.S., Rylander, D., Ohlin, K.E., Lundblad, M., Cenci, M.A., 2007. The "motor complication syndrome" in rats with 6-OHDA lesions treated chronically with L-DOPA: relation to dose and route of administration. Behav Brain Res 177, 150–159.
Lipski, J., Nistico, R., Berretta, N., Guatteo, E., Bernardi, G., Mercuri, N.B., 2011. L-DOPA: a scapegoat for accelerated neurodegeneration in Parkinson's disease? Prog Neurobiol 94, 389–407.
Martin, R.F., Bowden, D.M., 2000. Primate Brain Maps: Structure of the Macaque Brain. Elsevier.
Martinez, A.A., Morgese, M.G., Pisanu, A., Macheda, T., Paquette, M.A., Seillier, A., Cassano, T., Carta, A.R., Giuffrida, A., 2015. Activation of PPAR gamma receptors reduces levodopa-induced dyskinesias in 6-OHDA-lesioned rats. Neurobiol Dis 74, 295–304.
Mastroeni, D., Grover, A., Leonard, B., Joyce, J.N., Coleman, P.D., Kozik, B., Bellinger, D.L., Rogers, J., 2009. Microglial responses to dopamine in a cell culture model of Parkinson's disease. Neurobiol Aging 30, 1805–1817.
McGeer, P.L., Itagaki, S., McGeer, E.G., 1988. Expression of the histocompatibility glycoprotein HLA-DR in neurological disease. Acta Neuropathol (Berl) 76, 550–557.
Mercuri, N.B., Bernardi, G., 2005. The "magic" of L-dopa: why is it the gold standard Parkinson's disease therapy? Trends Pharmacol Sci 26, 341–344.
Milior, G., Lecours, C., Samson, L., Bisht, K., Poggini, S., Pagani, F., Deflorio, C., Lauro, C., Alboni, S., Limatola, C., Branchi, I., Tremblay, M.-E., Maggi, L., 2016. Fractalkine receptor deficiency impairs microglial and neuronal responsiveness to chronic stress. Brain Behav Immun 55, 114–125.
Montioli, R., Voltattorni, C.B., Bertoldi, M., 2016. Parkinson's Disease: Recent Updates in the Identification of Human Dopa Decarboxylase Inhibitors. Curr Drug Metab 17, 513–518.
Morin, N., Jourdain, V.A., Di Paolo, T., 2014. Modeling dyskinesia in animal models of Parkinson disease. Exp Neurol 256, 105–116.
Mulas, G., Espa, E., Fenu, S., Spiga, S., Cossu, G., Pillai, E., Carboni, E., Simbula, G., Jadžić, D., Angius, F., Spolitu, S., Batetta, B., Lecca, D., Giuffrida, A., Carta, A.R., 2016. Differential induction of dyskinesia and neuroinflammation by pulsatile versus continuous l-DOPA delivery in the 6-OHDA model of Parkinson's disease. Exp Neurol 286, 83–92.
Nayak, D., Roth, T.L., McGavern, D.B., 2014. Microglia Development and function. Annu Rev Immunol 32, 367–402.
Niraula, A., Sheridan, J.F., Godbout, J.P., 2017. Microglia Priming with Aging and Stress. Neuropsychopharmacology 42, 318–333.
Oertel, W., Eggert, K., Pahwa, R., Tanner, C.M., Hauser, R.A., Trenkwalder, C., Ehret, R., Azulay, J.P., Isaacson, S., Felt, L., Stempien, M.J., 2017. Randomized, placebo-controlled trial of ADS-5102 (amantadine) extended-release capsules for levodopa-induced dyskinesia in Parkinson's disease (EASE LID 3). Mov Disord Off J Mov Disord Soc 32, 1701–1709.
Ossola, B., Schendzielorz, N., Chen, S.-H., Bird, G.S., Tuominen, R.K., Männistö, P.T., Hong, J.-S., 2011. Amantadine protects dopamine neurons by a dual action: reducing activation of microglia and inducing expression of GDNF in astroglia [corrected]. Neuropharmacology 61, 574–582.
Pahwa, R., Tanner, C.M., Hauser, R.A., Isaacson, S.H., Nausieda, P.A., Truong, D.D., Agarwal, P., Hull, K.L., Lyons, K.E., Johnson, R., Stempien, M.J., 2017. ADS-5102 (Amantadine) Extended-Release Capsules for Levodopa-Induced Dyskinesia in Parkinson Disease (EASE LID Study): A Randomized Clinical Trial. JAMA Neurol 74, 941–949.
Pahwa, R., Tanner, C.M., Hauser, R.A., Sethi, K., Isaacson, S., Truong, D., Struck, L., Ruby, A.E., McClure, N.L., Went, G.T., Stempien, M.J., 2015. Amantadine extended release for levodopa-induced dyskinesia in Parkinson's disease (EASED Study). Mov Disord Off J Mov Disord Soc 30, 788–795.
Parent, A., Hazrati, L.N., 1995. Functional anatomy of the basal ganglia. I. The cortico-basal ganglia-thalamo-cortical loop. Brain Res Brain Res Rev 20, 91–127.
Perry, V.H., Nicoll, J.A.R., Holmes, C., 2010. Microglia in neurodegenerative disease. Nat Rev Neurol 6, 193–201.
Peters A, Palay SL, Webster H deF. 1991. The Fine Structure of the Nervous System. Neurons and their Supporting Cells. 3rd edition. J Neuropathol Exp Neurol 50:282–282.
Peterson, Lynda J., Flood, Patrick M., 2012. Oxidative Stress and Microglial Cells in Parkinson's Disease. Mediators of Inflammation 2012, 1–12. https://doi.org/10.1155/2012/401264.
Poewe, W., Antonini, A., Zijlmans, J.C., Burkhard, P.R., Vingerhoets, F., 2010. Levodopa in the treatment of Parkinson's disease: an old drug still going strong. Clin Interv Aging 5, 229–238.
Prigione, A., Begni, B., Galbussera, A., Beretta, S., Brighina, L., Garofalo, R., Andreoni, S., Piolti, R., Ferrarese, C., 2006. Oxidative stress in peripheral blood mononuclear cells from patients with Parkinson's disease: negative correlation with levodopa dosage. Neurobiol Dis 23, 36–43.
Riahi, G., Morissette, M., Samadi, P., Parent, M., Di Paolo, T., 2013. Basal ganglia serotonin 1B receptors in parkinsonian monkeys with L-DOPA-induced dyskinesia. Biochem Pharmacol 86, 970–978.
Sabens, E.A., Distler, A.M., Mieyal, J.J., 2010. Levodopa deactivates enzymes that regulate thiol-disulfide homeostasis and promotes neuronal cell death: implications for therapy of Parkinson's disease. Biochemistry 49, 2715–2724.
Sabens, E.A., Steller, K.M., Mieyal, J.J., 2011. Levodopa Activates Apoptosis Signaling Kinase 1 (ASK1) and Promotes Apoptosis in a Neuronal Model: Implications for the Treatment of Parkinson's Disease. Chem Res Toxicol 24, 1644–1652.
Sanchez-Guajardo, V., Febbraro, F., Kirik, D., Romero-Ramos, M., 2010. Microglia Acquire Distinct Activation Profiles Depending on the Degree of α-Synuclein Neuropathology in a rAAV Based Model of Parkinson's Disease. Available from:. PLoS ONE [Internet] 5.
Schapira, A.H., Jenner, P., 2011. Etiology and pathogenesis of Parkinson's disease. Mov Disord Off J Mov Disord Soc 26, 1049–1055.
Siani F, Greco R, Levandis G, Ghezzi C, Daviddi F, Demartini C, Vegeto E, Fuzzati-Armentero M-T, Blandini F. 2017. Influence of Estrogen Modulation on Glia Activation in a Murine Model of Parkinson's Disease. Front Neurosci [Internet] 11. Available from: https://www.frontiersin.org/articles/10.3389/fnins.2017.00306/full.
Stefanova, N., Fellner, L., Reindl, M., Masliah, E., Poewe, W., Wenning, G.K., 2011. Toll-Like Receptor 4 Promotes α-Synuclein Clearance and Survival of Nigral Dopaminergic Neurons. Am J Pathol 179, 954–963.
St-Pierre, M.-K., Bordeleau, M., Tremblay, M.-È., 2019. Visualizing Dark Microglia. Methods Mol Biol Clifton NJ 2034, 97–110.
Streit, W.J., 2002. Microglia as neuroprotective, immunocompetent cells of the CNS. Glia 40, 133–139.
Streit, W.J., Walter, S.A., Pennell, N.A., 1999. Reactive microgliosis. Prog Neurobiol 57, 563–581.
Takagi, S., Hayakawa, N., Kimoto, H., Kato, H., Araki, T., 2007. Damage to oligodendrocytes in the striatum after MPTP neurotoxicity in mice. J Neural Transm Vienna Austria 1996 (114), 1553–1557.
Tansey, M.G., Goldberg, M.S., 2010. Neuroinflammation in Parkinson's disease: its role in neuronal death and implications for therapeutic intervention. Neurobiol Dis 37, 510–518.
Tay, T.L., Savage, J.C., Hui, C.W., Bisht, K., Tremblay, M., 2017. Microglia across the lifespan: from origin to function in brain development, plasticity and cognition. J Physiol 595, 1929–1945.
Theodore, S., Cao, S., McLean, P.J., Standaert, D.G., 2008. Targeted Overexpression of Human Alpha-Synuclein Triggers Microglial Activation and an Adaptive Immune Response in a Mouse Model of Parkinson Disease. J Neuropathol Exp Neurol 67, 1149–1158.
Tremblay, M.-E., Cookson, M.R., Civiero, L., 2019. Glial phagocytic clearance in Parkinson's disease. Mol Neurodegener 14, 16.
Tremblay M-È, Lowery RL, Majewska AK. 2010a. Microglial Interactions with Synapses Are Modulated by Visual Experience. PLoS Biol [Internet] 8. Available from: https://www.ncbi.nlm.nih.gov/pmc/articles/PMC2970556/.
Tremblay M-E, Riad M, Majewska A. 2010b. Preparation of Mouse Brain Tissue for Immunoelectron Microscopy. J Vis Exp JoVE [Internet]. Available from: https://www.ncbi.nlm.nih.gov/pmc/articles/PMC3156065/.
Tremblay, M.-È., Zettel, M.L., Ison, J.R., Allen, P.D., Majewska, A.K., 2012. Effects of aging and sensory loss on glial cells in mouse visual and auditory cortices. Glia 60, 541–558.
Tynan, R.J., Beynon, S.B., Hinwood, M., Johnson, S.J., Nilsson, M., Woods, J.J., Walker, F.R., 2013. Chronic stress-induced disruption of the astrocyte network is driven by structural atrophy and not loss of astrocytes. Acta Neuropathol (Berl) 126, 75–91.
Tysnes, O.-B., Storstein, A., 2017. Epidemiology of Parkinson's disease. J Neural Transm 124, 901–905.
Viceconte N, Burguillos MA, Herrera AJ, De Pablos RM, Joseph B, Venero JL. 2015. Neuromelanin activates proinflammatory microglia through a caspase-8-dependent mechanism. J Neuroinflammation [Internet] 12. Available from: https://www.ncbi.nlm.nih.gov/pmc/articles/PMC4302615/.
Vijayakumar, D., Jankovic, J., 2016. Drug-Induced Dyskinesia, Part 1: Treatment of Levodopa-Induced Dyskinesia. Drugs 76, 759–777.
Vyas S, Rodrigues AJ, Silva JM, Tronche F, Almeida OFX, Sousa N, Sotiropoulos I. 2016. Chronic Stress and Glucocorticoids: From Neuronal Plasticity to Neurodegeneration. Neural Plast [Internet] 2016. Available from: https://www.ncbi.nlm.nih.gov/pmc/articles/PMC4806285/.
Walker, F.R., Beynon, S.B., Jones, K.A., Zhao, Z., Kongsui, R., Cairns, M., Nilsson, M., 2014. Dynamic structural remodelling of microglia in health and disease: A review of the models, the signals and the mechanisms. Brain Behav Immun 37, 1–14.
Weenink, S.M., Gautam, A.M., 1997. Antigen presentation by MHC class II molecules. Immunol Cell Biol 75, 69–81.
Westermann, B., 2008. Molecular Machinery of Mitochondrial Fusion and Fission. J Biol Chem 283, 13501–13505.
Wu, D.C., Jackson-Lewis, V., Vila, M., Tieu, K., Teismann, P., Vadseth, C., Choi, D.-K., Ischiropoulos, H., Przedborski, S., 2002. Blockade of microglial activation is neuroprotective in the 1-methyl-4-phenyl-1,2,3,6-tetrahydropyridine mouse model of Parkinson disease. J Neurosci Off J Soc Neurosci 22, 1763–1771.
Xu, S., Chan, P., 2015. Interaction between Neuromelanin and Alpha-Synuclein in Parkinson's Disease. Biomolecules 5, 1122–1142.
Zecca, L., Wilms, H., Geick, S., Claasen, J.-H., Brandenburg, L.-O., Holzknecht, C., Panizza, M.L., Zucca, F.A., Deuschl, G., Sievers, J., Lucius, R., 2008. Human neuromelanin induces neuroinflammation and neurodegeneration in the rat substantia nigra: implications for Parkinson's disease. Acta Neuropathol (Berl) 116, 47–55.

Zhang, W., Phillips, K., Wielgus, A.R., Liu, J., Albertini, A., Zucca, F.A., Faust, R., Qian, S.Y., Miller, D.S., Chignell, C.F., Wilson, B., Jackson-Lewis, V., Przedborski, S., Joset, D., Loike, J., Hong, J.-S., Sulzer, D., Zecca, L., 2011. Neuromelanin activates microglia and induces degeneration of dopaminergic neurons: implications for progression of Parkinson's disease. Neurotox Res 19, 63–72.

Zhao, C., Ling, Z., Newman, M.B., Bhatia, A., Carvey, P.M., 2007. TNF-Alpha Knockout and Minocycline Treatment Attenuates Blood Brain Barrier Leakage in MPTP-Treated Mice. Neurobiol Dis 26, 36–46.

Zotova, E., Bharambe, V., Cheaveau, M., Morgan, W., Holmes, C., Harris, S., Neal, J.W., Love, S., Nicoll, J.A.R., Boche, D., 2013. Inflammatory components in human Alzheimer's disease and after active amyloid-β42 immunization. Brain J Neurol 136, 2677–2696.